Geophysical Methods for Detecting Permafrost Discontinuities

by

Max Salman

A thesis
presented to the University of Waterloo
in fulfilment of the
thesis requirement for the degree of
Master of Applied Science
in
Civil Engineering

Waterloo, Ontario, Canada, 2021

Author's Declaration

I hereby declare that I am the sole author of this thesis. This is a true copy of the thesis, including any required final revisions, as accepted by my examiners.

I understand that my thesis may be made electronically available to the public.

Abstract

Global climate change has sparked various concerns over the future of the Arctic. One of the major concerns around the environmental and ecological health of the Arctic is directly related to the deterioration of the permafrost. Permafrost is described as frozen soil below 0°C for at least two consecutive years, and is recognized by the World Meteorological Organization (WMO) as an Essential Climate Variable (ECV). Geophysical methods have been used to detect and measure the extent of the permafrost in various cold regions of the Earth. Traditional methods such as electrical resistivity tomography (ERT), electro magnetic induction (EMI), and seismic have all been used to characterize permafrost in the subsurface. However, there are smaller scale features at the near surface requiring attention. In this work, we used of a permafrost probe, an electrical resistivity tomography system, and an electromagnetic induction system to measure the depth to the permafrost table from the ground surface. The study was performed in the Sahtu Region of the Northwest Territories, approximately 30 kilometers south of the Town of Norman Wells, Northwest Territories.

Two sites were selected; one on a drill pad, one near a lake shore. The soils mainly consisted of homogeneous organic-rich till. The permafrost probe measure a depth to permafrost table of approximately 70 centimeters at the drill-pad site (MW04T) and approximately 30 centimeters at the lake shore site (Marg Lake). A Syscal Junior 48^{TM} ERT system was installed perpendicular to the topological features, such as the lake shore, and the tree line. The electrode spacing was small due to the shallow nature of the permafrost, and the dipole-dipole method was selected to collect measurements. The ERT data was inverted using Res2DInv^{TM} and the output data correlates well with the permafrost probe measurements. A ground conductivity meter (GCM) was used to assess the capability of using a non-ground-coupled geophysical methods in this terrain to detect permafrost discontinuity. We deployed the Geonics EM-31^{TM} and EM-34^{TM} systems. The electrical data was collected over the same permafrost probe and ERT survey lines and measurements were plotted using MATLAB^{TM}. The data suggest that the GCM systems were able to effectively detect the change in permafrost table depth, correlative todirect measurement of permafrost depth that were used concurrently. This study serves as a baseline analysis of using small-scaled ground-based geophysical systems to detect permafrost discontinuities in this region, and informs the future development of aerial-based systems and methods to gather multiple strings of data to estimate permafrost table depth, and the integrity of the permafrost.

Acknowledgements

+JMJ

I want to begin by thanking God for Blessing me with the motivation to pursue meaningful research that impacts the world so that the quality of human life and the Earth is continuously recognized and enhanced.

The University of Waterloo administration has been supportive throughout my academic career and have shared with me great insight on my next steps beyond this project. I am grateful for their friendship and support, especially through times of trial.

I am very thankful to Dr. James Craig, who has graciously accepted to work with me and guide me in the final stages of this document. I appreciate the guidance I have received over the past seven months.

To my friends and graduate student colleagues: I am incredibly grateful for your friendship and support during this difficult time. Many of you have lent a listening ear to the struggles I have faced during this process. You have given me encouragement by example, and by kind words.

Funding for the first two years of this project was provided from the Global Water Futures program.

Access to the field site in 2018 was provided by Husky Energy.

Colby Steelman showed me the simple operation of Res2DInv.

David Rudolph and Aaron Vandenhoff assisted in equipment handling and data collection.

Dedication

+JMJ

I dedicate this document to all graduate researchers, whom during their graduate careers, suffered harassment or academic neglect from their faculty advisor.

Quote

"What can not be measured, can not be managed"
- Amr

Territorial Acknowledgement

The Waterloo, Kitchener, and Cambridge campuses of the University of Waterloo are situated on the Haldimand Tract, land that was promised to the Haudenosaunee of the Six Nations of the Grand River, and are within the territory of the Neutral, Anishinaabe, and Haudenosaunee peoples.

The various data collected for this work are from the Sahtu Region of the Northwest Territories, and also acknowledge the Indigenous history of that territory.

Table of Contents

List of Tables

List of Figures

Chapter 1

Introduction

Climate change is one of the most important issues in modern times, and requires much attention as it affects the quality of life of humans and the surrounding ecosystem. Understanding processes that enhance and accelerate climate change can provide insight on mitigation strategies. One of the critical impacts of climate change in the North is the thawing of permafrost, which has repercussions on the livelihoods of northern communities, northern development, geotechnical projects and also can lead to increased CO_2 in the atmosphere.

Global climate change has sparked various concerns over the future of the Arctic. One of the major concerns around the environmental and ecological health of the Arctic is directly related to the deterioration of the permafrost. Permafrost is described as frozen soil below 0^oC for at least two consecutive years, and is recognized by the World Meteorological Organization (WMO) as an Essential Climate Variable (ECV). Geophysical methods have been used to detect and measure the extent of the permafrost in various cold regions of the Earth. Traditional methods such as electrical resistivity tomography (ERT), electro magnetic induction (EMI), and seismic tomography have all been used to characterize permafrost in the subsurface. However, there are smaller scale features at the near surface requiring attention. Features such as creeks, small lakes and clear-cutting of a forest can be associated with permafrost disturbance.

Technological breakthroughs in the geosciences give access to the tools necessary to collect new measurements that may be relevant to scientific investigation of permafrost. This research will focus on using geophysical methods to identify the presence or absence

of permafrost in northern landscapes. Geophysics is the sub-domain of the geosciences that measures the physical characteristics of the Earth to understand subsurface properties of the region of investigation. These methods, which are based upon indirect observations of gravity, magnetics, radiometrics and electromagnetics, are often non-invasive in nature, and can be mounted on aircraft to collect measurements remotely. Mapping permafrost at a high resolution is useful for engineers building roads and other subterranean infrastructure, is important for climate scientists to understand small-scale processes causing the thaw and regeneration of permafrost, and for northern agriculture, better estimate where lands are suitable for farming.

1.1 Objective Statement

The objective of this work is to use a pilot set of data from non-ground-coupled geophysical equipment to detect permafrost discontinuity under conditions where the ground surface has undergone anthropogenic or natural changes, for example tree clearings or lake shores. The field site is located in the Sahtu Region of the Northwest Territories in Canada. The area contains large extents of discontinuous permafrost and surface water features are indicative of potential vertical groundwater/surface water interactions. This work is intended to operate as a proof of concept for an aerial drone-based geophysical system. Current airborne geophysical measurement methods involve large helicopters and fixed-wing aircraft that have two pilot/operators, which is expensive and inefficient since these vehicles require an airport, or suitable landing area. Using small remotely piloted aerial systems (RPAS), only a ground-based operator is required to accomplish the survey.

The use of this method has practical applications for engineering purposes including road construction, risk assessment, and identifying slump prone zones. The research will give insights into monitoring permafrost thaw to address climate change as it relates directly to permafrost degradation and hydrogeologic conditions of cold regions, particularly in very remote and hard to access areas and landscapes. The vision is to establish a monitoring and surveying method that is efficient enough for end-users to gather data using remote techniques, whereby in difficult or dangerous landscapes, data can be gathered and collected for use to monitor high sensitivity regions. Electrical Resistivity Tomorgraphy has been used already to detect permafrost, however, requires physically installing equipment into the soil. As will be presented in this work, other electrical methods such as electromagnetic induction does not require any ground disturbance and can generate ideal results for geoscientists to interpret. This method can also be equipped on aircraft to

account for more ground clearance if necessary.

Chapter 2

Literature Review

2.1 Importance of Permafrost

Northern cold regions and the Arctic are susceptible to rising temperatures due to climatic change and there is a common agreement that the global mean annual temperature is increasing [10]. Northern regions, particularly Northern Canada, the High Arctic and Northern Asia, are permafrost rich in the substrata. Permafrost is defined as ground that is below 0°C for at least two consecutive years. The susceptibility to thawing and subsequent melting of the permafrost in the Northern Regions is resulting in the general deterioration of Arctic permafrost [9]. This in turn affects the physical hydrogeological properties on a vast regional scale [3], contributing to ecological change in these areas [25].

This literature review provides background information on geophysical and some remote sensing techniques and methods that have been successfully deployed to observe permafrost discontinuity. This will provide context for this work with relation to previous research efforts. Subsequently, as a product of this review, the applicability of currently deployed methods is examined and compared to non-geophysical techniques.

2.1.1 Discontinuous Permafrost in the Central Mackenzie Valley

The Central MacKenzie Valley is located in a discontinuous permafrost zone in the Canadian Arctic, as evident in Figure 2.1. The instances of irregular permafrost affect various

landscape changes in the region. Some examples include thaw slumps, land elevation variation, and vegetation variation, some of which may be identified using remote sensing. The presence or absence of permafrost in some cases is not visible from conventional remote sensing. Use of geophysical monitoring could help identify, for example, absence of permafrost as a precursor of thaw slumping.

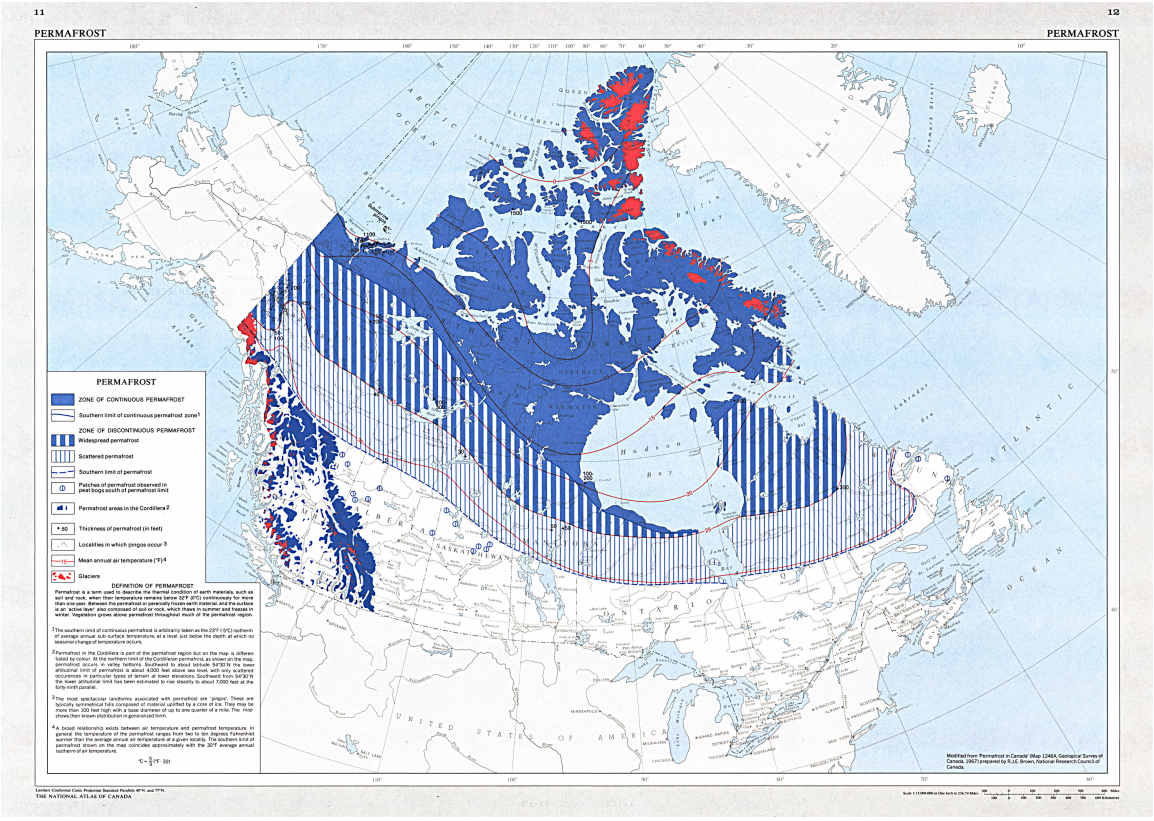

Figure 2.1: Map of Canadian permafrost conditions (NRCan 1967)

A major federal project to better understand the permafrost conditions in the Mackenzie Valley main corridor was conducted and a report was published by the National Research Council of Canada in 2010. The report outlined the extent of permafrost, the active layer thicknesses and demonstrates the vulnerability of the area. Several vertical temperature profiles were created to map the temperature conditions, whereby the authors conclude that the permafrost in the region is near the 0°C mark, and that minor variations in temperature can have a significant impact on the integrity of the permafrost [17]. Work

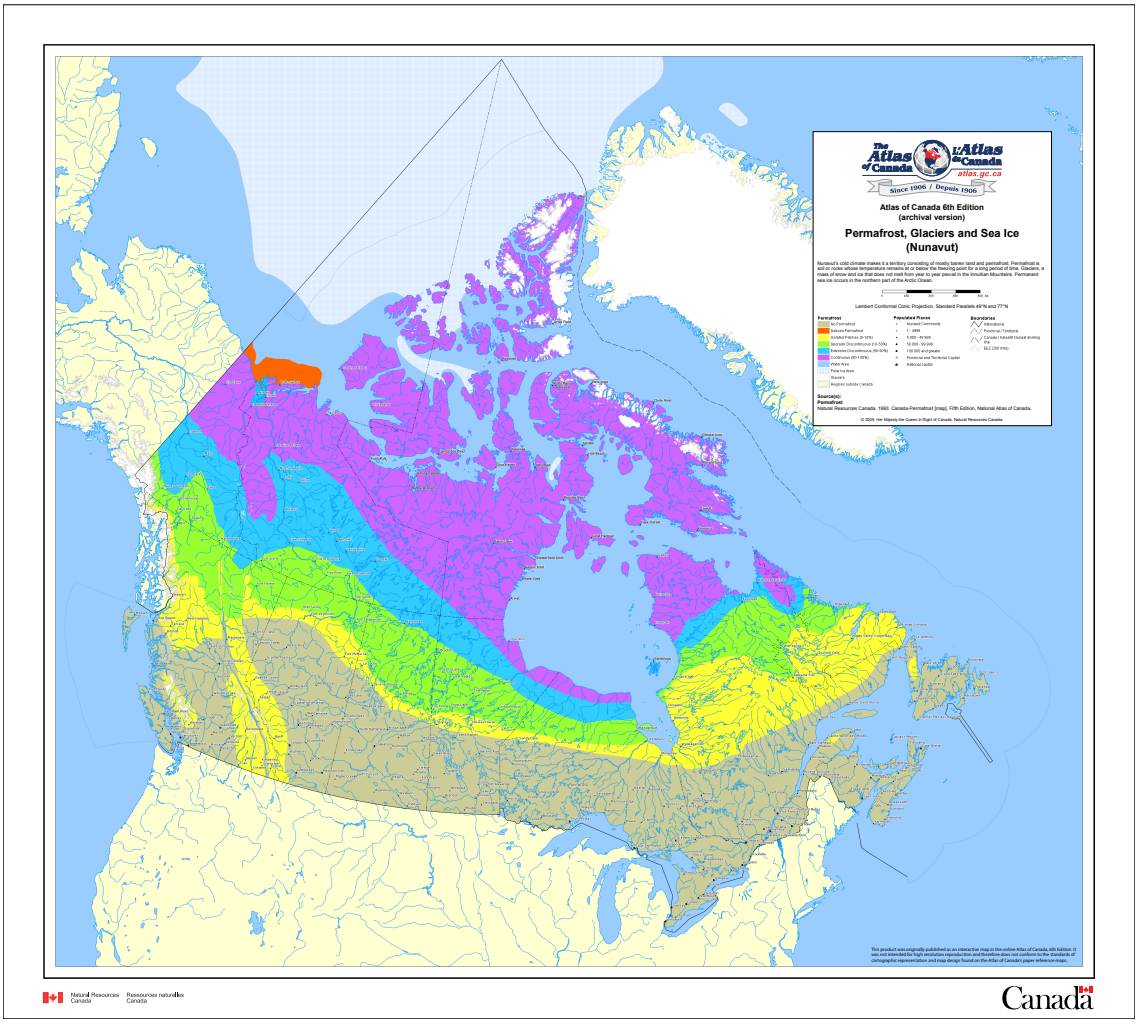

Figure 2.2: Map of Canadian permafrost conditions (NRCan 2009)

by Burgess and Smith (2001) provides some insight on the relationship between the Mean Annual Air Temperature (MAAT) and the Mean Annual Ground Temperature (MAGT) in region [2]. The following MAAT/MAGT relationship is represented as:

$$\text{MAGT} = 0.68 \cdot \text{MAAT} + 2.96 \quad \text{R}^2 = 0.44 \tag{2.1}$$

The dynamic nature of the unfrozen water, be it derived from permafrost, or residing in the active zone, is related to the temperature of the water inducing a thermal gradient

furthering the permafrost deterioration, and consequently leading to enhanced groundwater flow [13]. Meanwhile, the temperature gradient also propagates through the liquid water, and drives convection-based flow, where under ideal conditions, is limited to vertical flow [5]. However, while liquid water is mobile, the heat of the water may be transported laterally and can expedite permafrost thaw.

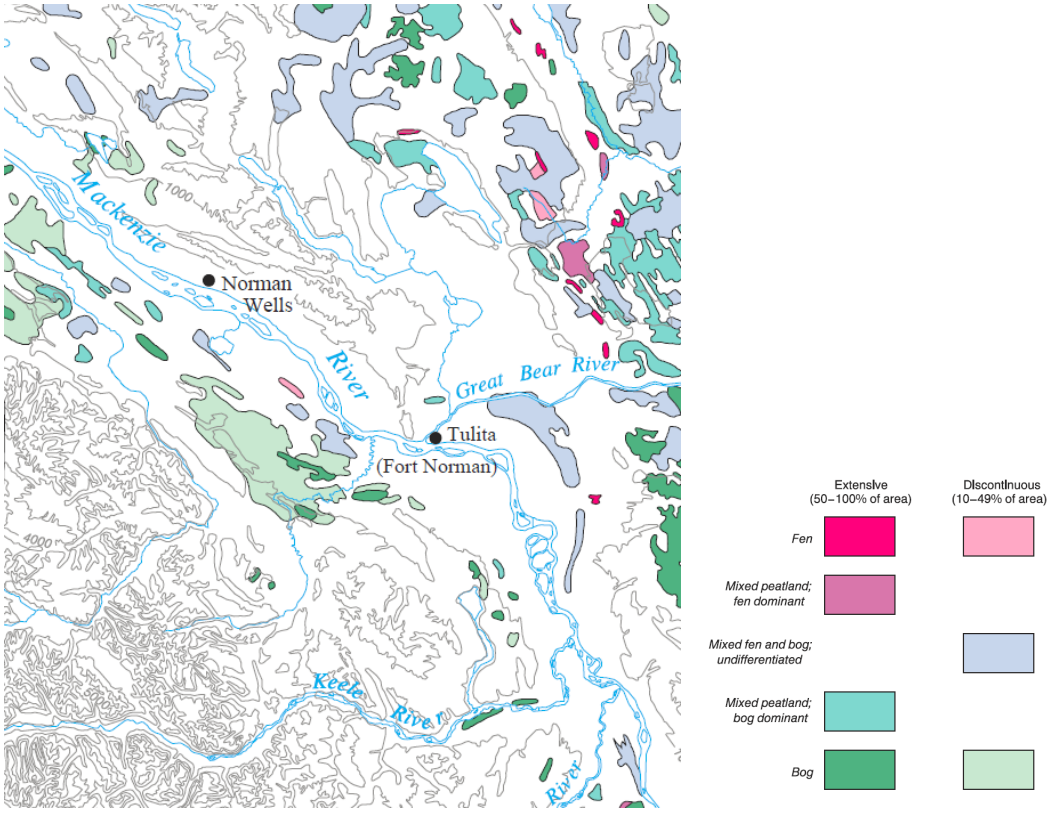

Figure 2.3: The distribution of fens and bogs in the field site, modified for scale from J.M. Aylsworth (NRCan 1996)

2.1.2 Impacts on Engineering Efforts

Given the physical properties of permafrost in soils, and the drastic change in geotechnical properties upon its thawing, the dynamics of permafrost thaw as a consequence of natural or human activity have an impact on engineering projects. For example, road infrastructure is highly affected by thawing permafrost due to the impact on the road bed integrity [24].

On alpine or sloped environments, the thawing of permafrost can lead to instability due to increased groundwater mobility [22, 7]. Because of issues like these, it is paramount to develop efficient systems that can monitor the permafrost integrity at a scale that is appropriate to infrastructure. To this effect, it is also very important to understand the amounting impacts of human activity on permafrost continuity, and the consequences of modifying landscapes in permafrost rich areas. One of the more sever impacts of permafrost thaw is the genesis of thermokarst and slumping [19], which has obvious repercussions on infrastructure, but can also present major challenges for Indigenous groups in permafrost rich regions [15], such as the negative impacts on ecosystems, or traditional practices in their territories and lands.

2.2 Direct Permafrost Measurement

To get a direct measurement of the top of the permafrost, permafrost probes are typically used in the field. A permafrost probe is a steel rod with a perpendicular handle that is manually driven into the ground until it strikes the permafrost table. Permafrost probes have several drawbacks however. This requires manual labour, and is dependent on the user. Through dense soils, a weaker operator may not be capable of penetrating the soil. The soil may also have rocks within it, whereby a reading may be falsely interpreted as a result of striking a rock or other hard object in the ground. Permafrost probes are also limited in length. Longer probes can be available, however become tedious to remove from soils once penetrated within. For shallow permafrost, these probes can be appropriate, however, a permafrost probe that is designed to be operated at shoulder height can only reach 1.5 meters. Therefore, the maximum measurement depth of the probe is dependent on the length of the probe itself. Furthermore, it only allows the operator to measure the top of the permafrost, without any information about permafrost thickness.

Thermistors can also provide a direct measurement of permafrost depth and thickness. Since permafrost is soil that is at or below zero degrees Celsius, temperature measurements can be taken to detect where the soil is below freezing. Thermistor measurements can be automated and delivered over-the-air (OTA) using a cellular network or satellite data connection. There are however significant drawbacks to this method. Termistor strings can only provide the temperature at the point at which the thermistor is installed. For example, a vertical installation of thermistors will only provide a vertical temperature profile for a single point on a two dimensional surface. Installation of a thermister string also requires drilling. Dependent on location, drilling services may be infeasible. This can make

direct permafrost measurements highly costly, and unattainable for many researchers and northern communities.

In-situ measurements of permafrost depth are labour-intensive. They usually involve large equipment requiring a significant mobilization effort. The equipment is expensive to manufacture and transport, and may require more than two personnel. Beyond the logistical issues concerning this large equipment, the size and process may require forest clear-cutting, explosives, and power generation using diesel or gasoline.

2.3 Use of Remote Sensing Data

Remote and optical sensing provide the opportunity to detect and possibly quantify the lateral extent of permafrost degradation from afar without use of geophysical techniques. Remote sensing measurements of the earth's surface are used for hazard detection and prediction [8], which can be useful, as an example, this can be used to assess the risk of thaw slumps. Satellite and high-level remote sensing, such products as NASA's Landsat™ and Planet Labs™ provide adequate resolution imagery to detect geomorphological changes at surface level that may be characteristic of permafrost degradation. The presence of landscape features such as fens and bogs may also be indicative of permafrost presence or absence [26].

Where lateral temperature gradients are steep, thermal infrared (IR) is a near-optical geophysical method that can be used to detect the spatial distribution of ground surface temperature. This method has been applied in the air and ground to monitor groundwater/surfacewater interactions [14]. Unfortunately, ground temperature does not perfectly correlate to subsurface temperature, and therefore infrared is of limited use in determining the presence of permafrost.

Satellite-based remote sensing can be very useful to identify candidate sites that may be experiencing permafrost thaw, or to be directly applied to assessment of thaw at relatively large scales. Remote sensing data is almost always spatial, rarely temporal only, and the nature of the data should be such that the information analysed shows a form of variation over an area, or over a length of time, respectively. The variation can be anthropogenic, or natural. The landscape or time anomalies can be collected visually, or by other methods as are described in this section.

Satellite and high altitude remote sensing provides increasingly detailed geomorphological data that can assist in investigating regions of interest. General optical imagery is available from the United States Geological Survey (USGS) and non-governmental sources such as Google Maps™.

Use of satellite and high altitude airborne remote sensing to assess physical conditions of the Earth's surface has been instrumental in making informed decisions about the environment, and to monitor changes, for instance, topographical changes are detected and result in potentially invasive surface and subsurface measurements to gather higher precision information about the surficial changes and to collect subsurface data. This means that, although remote sensing may provide some information related to permafrost thaw, it is better supported with more evidence traditionally using ground-based techniques, which may result in the destruction of the landscape and subsequently the ecosystem.

Work has been done using satellite-based remote sensing to estimate the vegetation in the Mackenzie Delta as a result of permafrost conditions [12]. Note the field site, in Figure 2.4, is located along various waterways, and includes small to large lakes. Although not directly the purpose of this work, it is another method that uses vegetation cover as a proxy to permafrost thaw. Ocassionally, the visual aid of remotely acquired data, and by means of processing the data to solve for some key identifiers of permafrost thaw, such as vegetation type and height, a data set can be compiled to infer a suitable geophysical survey site. Figure 2.4 indicates the inferred permafrost zone.

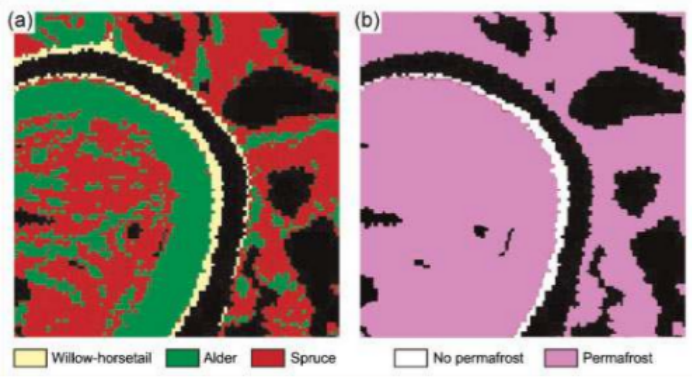

Figure 2.4: Processed remote sensing image of a meandering river in the Mackenzie Delta. (Nguyen 2009)

Preferential vegetation growth can be closely associated to groundwater flow direction, any contamination in the groundwater, or is stressed by a potentially lowering water table

[23]. Knowledge of vegetation as it relates to permafrost distribution is not a novel concept. Research by Dingman and Koutz (1974) demonstrates the effects of vegetation change and loss on the state, and fate, of permafrost. Additionally, canopy cover hinders the blocking of snow, which acts as an insulator in cold regions. As the snow pack is thicker, the spring and summer thermal energy is trapped in the soil, and consequently retains the heat near the permafrost table, thus potentially contributing to the growth of the active zone [4]. These snow packs, and zones of low canopy cover can suggest suitable survey sites to look at the change in permafrost conditions. Soil moisture or springs based on satellite and airborne imagery can be inferred as a shallow water table [11]. Combining visual imagery where near-surface groundwater can be seeping to the surface and infrared information, one could ideally locate where groundwater discharge is occurring. Ground temperature based on infrared measurements may also be an indicator of the presence of groundwater or permafrost. The lower temperature of permafrost compared to the temperature of near surface groundwater is typically apparent on an infrared map.

Satellite and aerial remote sensing techniques are not limited to visualizing tree cover, other bands can provide information relevant to permafrost such as temperature. To measure ground surface temperature, thermal infrared methods can be used to detect warmer zones on the Earth's surface. Integrating this information with visual band data is beneficial.

The use of remote sensing is limited to the spatial coverage of satellites, and satellite imagery can be lower spatial resolution than direct or indirect permafrost measurements, such as permafrost probe measurements, or electrical geophysical methods (example electrical resistivity tomography). Additionally, remote sensing measurements are reliant on ground surface characteristics, subsurface characteristics are inferred as a result. Additionally, collected data may be available for purchase, however independent data collection can be difficult to impossible if satellite-based. Use of aircraft is very expensive, but remotely piloted aerial systems (RPAS) are becoming increasingly available for low-altitude remote sensing.

It is important and necessary to acknowledge reconciliation efforts in Canada seeking to engage Indigenous peoples to contribute in the form of Indigenous Knowledge (IK). The term is not novel and is used in science to represent knowledge that is transmitted using traditional Indigenous methodology, such as ceremonials, story telling, and religious activities. This historical data can provide temporal and spatial data such that it can help inform research initiatives by providing pre-colonial era information [1]. Land cover change

has been mapped by means of satellite imagery combined with IK, see Rees et al (2003), the IK was sources from surveys of the people, and local and regional administrative offices [16].

2.4 Overview of Current Geophysical Methods

2.4.1 Electrical Methods

Electrical methods such as ground penetrating radar, electrical resistivity tomography, and electromagnetic induction are alternates to direct measurements of remote sensing methods for detecting permafrost. Figure 2.5 demonstrates the various methods that have been recently deployed and their respective scales and depths of investigation.

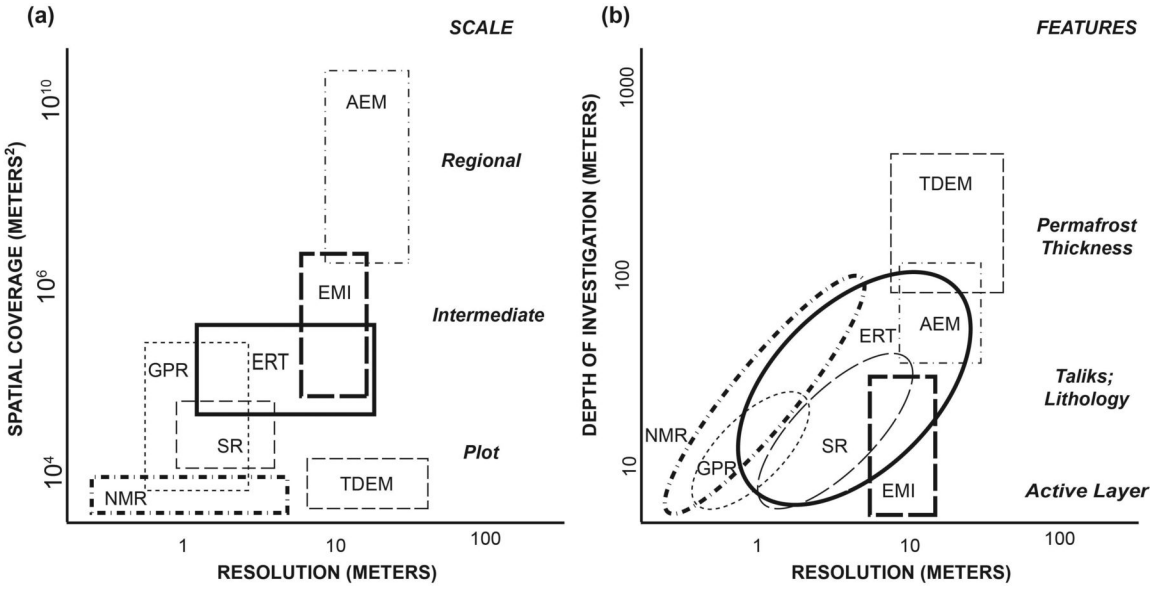

Figure 2.5: Plots showing geophysical methods for assessing permafrost and their respective scales, resolutions, and depths of investigations. (Walvoord 2016)

The scales at which ground-based electrical geophysical equipment operate is ideal for the work performed in this study, however the literature strongly suggests that the applications of airborne electrical equipment for smaller scaled surveys are rare [22].

2.4.2 Seismic

Seismic tomography uses a source that generates a vibration that penetrates through the ground, and the generated waves reflect and refract at interfaces between porous media with different acoustic properties. These reflections are recorded using geophones, that measure the amplitude of the vibrations of the ground. This method can be used to survey great depths. The application of large-scale seismic geophysics normally involves large machinery, vibrating trucks or explosives, and requires the clear-cutting of forests to provide the necessary access for this equipment.

2.4.3 Electrical Resistivity Tomography

Techniques have been deployed in the past few decades to map the contrasting ice and water content in the ground by electrical resistivity tomography (ERT). ERT uses electrodes to induce an electric current into the ground. The voltage and current are measured at the electrodes, and a resistivity is calculated and recorded by the system's computer. ERT surveys identify permafrost as highly resistive areas in contrast to unfrozen and more conductive media [10]. Although measurements are made at the electrode pairs, the estimated resistivity is a bulk measurement of the media between the two electrodes. This method requires ground coupling, and is generally quite heavy and tedious to mobilize. The electrodes must be equally spaced and fully inserted into the soil. Modern ERT surveys are autonomously run by a central computer system, only once the equipment has been fully installed.

2.4.4 Electromagnetic Induction

Techniques such as time domain, and frequency domain electromagnetic induction (TDEM and FDEM respectively) are being used to measure the electrical conductivity and resistivity of the subsurface [18], which can often be correlated to the presence or absence of permafrost. FDEM-EMI uses a transmitter coil and a receiver coil. The transmitter coil is always 'on'. The electromagnetic field, generated by the transmitter coil, is continuously monitored by the receiver coil and its recording device. As the system is moved laterally along the ground surface, the strength of the electromagnetic field changes proportional to the local resistivity of the soil. TDEM-EMI uses the same electromagnetic principle at FDEM, however rather than a constant transmission of the electromagntic field, the transmitter emits electromagnetic pulses. When the transmitter is emitting a pulse, this is

called the "on-time". The receiver measures and records the resulting electromagntic field when the transmitter is not emitting a pulse, also known as the "off-time" EMI methods can be implemented in the ground or in the air, as airborne electromagnetics (AEM). EMI does not require the equipment to be installed onto or into the ground.

Applying the principles of EMI and ERT has yielded a similar product to the CGG Resolve^{TM} airborne system, namely Capacitively-Coupled Resistivity (CCR), which uses various coil sizes and separations to simultaneously measure resistivity at various depths. The Geometrics OhmMapper^{TM} is a ground-based CCR system that has been used to map the the top of the permafrost table in cold regions [6]. The latter method requires the device to be coupled to the ground and can not be deployed onto an airborne platform.

2.4.5 GPR - Icing Detection

Ground Penetrating Radar (GPR) is used in several applications where permafrost and physical characteristics of permafrost rich or degraded regions are assessed[20, 21]. This can be a suitable method for detecting icings below a snowpack. Icings are smooth ice formations on the ground surface as a result of groundwater discharge during cold seasons. The difference in dielectric permitivity between ice and water can provide information about the location of the permafrost table. Considerations when selecting an appropriate GPR system depend on the desired depth of investigation, and the assumed the thickness of the individual geological layers in the subsurface. High frequency GPR systems can detect smaller features and are generally more sensitive to the change of dielectric permitivity through a medium. There are however drawbacks to using high frequency GPR for icing detection. For example, the signal's shorter wavelength suffers from energy losses at near surface as the generated wavelets are reflected and scatter more, this means it has a shallower penetration depth. That being said, for shallow permafrost, the high frquency equipment, when operated from the ground can display the depth of the permafrost table. Conversely, the longer wavelength, low frequency system generates a transmission that carries greater energy and will likely intercept the major ice and snow units. This technique is also applicable to investigate the major cryostratigraphic units within the sediment base to see whether preferential groundwater channels are present.

Chapter 3

Site Characteristics

The field site is located in the Sahtu Region of the Northwest Territories in sub-Arctic Canada, adjacent to the northward flowing Mackenzie River in the Central Mackenzie Valley. It is located approximately 30 kilometres South of Norman Wells (65°16'52"N 126°49'53"W). The region is characterized as having discontinuous permafrost with shallow groundwater. The terrain is uneven and inaccessible by a conventional automobile. The area located in the Boreal Biome and is vegetated densely with Balsam Fir, Tamarack, White Spruce, Black Spruce, and Jack Pine. The surface is a rugged hummocky terrain typical of the northern regions of the Northwest Territories and Nunavut's Tundra. There are small lakes dispersed throughout the region, their layout and shapes are noticeably parallel to one another, with creeks that run parallel and orthogonal to one another. This region is approximately 30 kilometers southwest of the Town of Normal Wells, and can be accessed via an ice road in the winter, or is limited to sea or air access in the Summer. The area is developed as a consequence of oil discovery. Crude light oil was found dissipating through the sediment into the Mackenzie river. The region is situated in the lowlands to the East of the Mackenzie Mountains, West of Great Bear Lake, and North of the Franklin Mountains.

3.1 Field Site Geology

Glacial processes dominate the physical landscape of the region, and a glacial depositional environment at the base of the vegetation. In the region, sand, till, and clay, are all present and contribute to the diverse soils of the area. The geology of the area is anticlinal in nature, and is a member of the Cordilleran Orogeny. The geological information has been

accessed through the GEOSCAN portal from the Government of Canada. The geological interpretation is based on the work of Fallas and McNaughton (2013), and, Cote et al (2013). The information is available to the public via the GEOSCAN portal by accessing http://geoscan.nrcan.gc.ca.

3.2 Surficial Geology

The vast majority of the Bogg Creek field site is overlain by till material. There is a very large linear feature of organically rich peat through the centre of the watershed that runs from the Northwest to the Southeast. To the East of the site, there is silt and sand. There is no bedrock outcrop in within the Bogg Creek watershed. Fens are characteristic of the northern part of the watershed. In the centre of the watershed, there is a small colluvium feature.

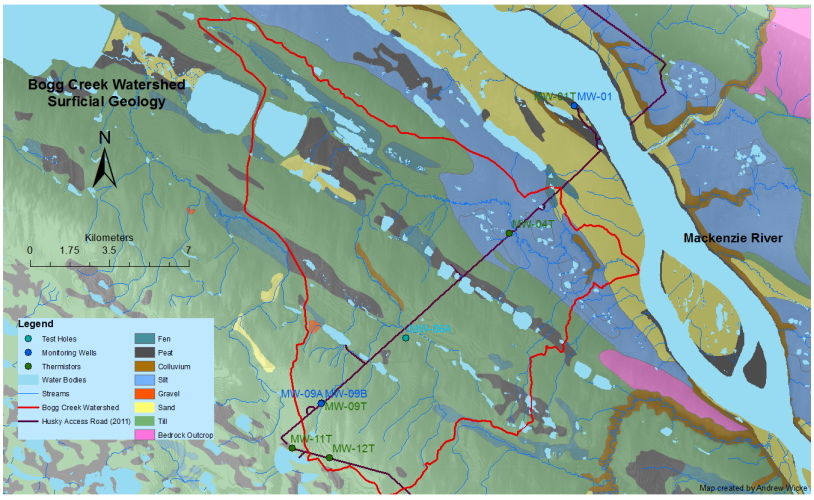

Figure 3.1: Surficial geology of the research site. Sahtu Region, NWT. (Wicke 2019)

3.3 Bedrock Geology

The bedrock geology of the Bogg Creek Watershed extends temporally from the Late Cretaceous to the Devonian with Quaternary sediments along the shores of the Mackenzie River and further to the southwest of the field site. Of the Late Cretaceous, both the

Little Bear Formation and the Slater River Formation are both present. The regional geological makeup is distributed in a relatively parallel fashion, and runs from the northwest to the southeast. The Quaternary sediments overlay the Little Bear Formation, which subsequently gives way to the Slater River Formation to the northeast. The Devonian Imperial Formation is the next major formation which backs onto the Mackenzie River. The interface between the Slater River Formation and the Imperial Formation has a pinching out band of the Arctic Red Formation and Martin House Formation. The Loon Creek Anticline strikes west northwest to east southeast over the Imperial Formation, and subsequently the Slater River Formation.

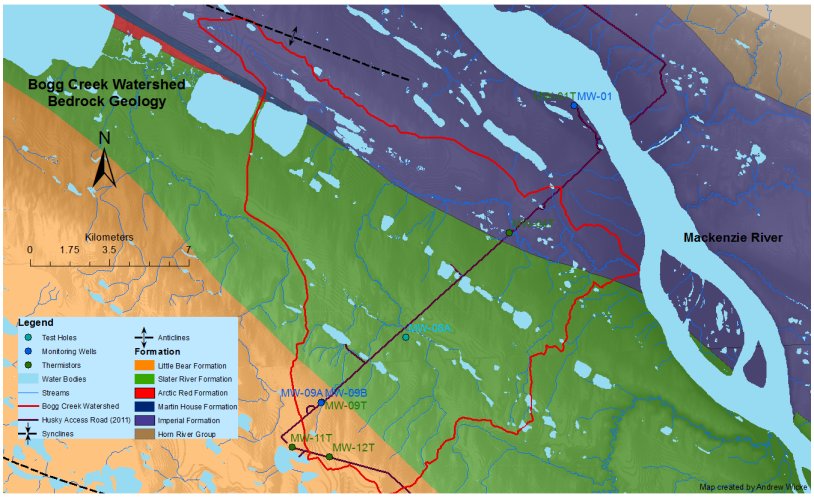

Figure 3.2: Bedrock geology of the research site. Sahtu Region, NWT. Source, (Wicke 2019)

3.4 Field Site Climate

Environment Canada data for 1981-2010 reports the average daily temperature in January to be -26°C, and July as 17°C, as the coldest and warmest months, respectively. Based on the same data, mean annual rainfall precipitation is 171 millimetres, where highest rainfall is in June, and mean annual snowfall precipitation is 161 centimetres, where greatest amount of snowfall is in October. Maximum average snow depth is reached in March, and is 30 centimetres. The average month end snow pack begins in October and ends in April or May. Climate data is based on measurements made at the Normal Wells Airport. The

precipitation contributes to both to surface and groundwater processes. Average yearly cloud cover is predominantly 80-100%, with greatest extent of cloud cover in October.

3.5 Temperature Measurements

Temperature measurements were collected at the drill pad site by Husky Energy. Thermister strings were installed and recorded. Figure 3.3 shows the vertical minimum and maximum temperature profiles at the site MW04T in 2014, 2015, and 2016. The plots indicate that the soil is warming enough to melt the ice content. However, the 2015 and 2016 data are limited to a depth of only 2.5 meters.

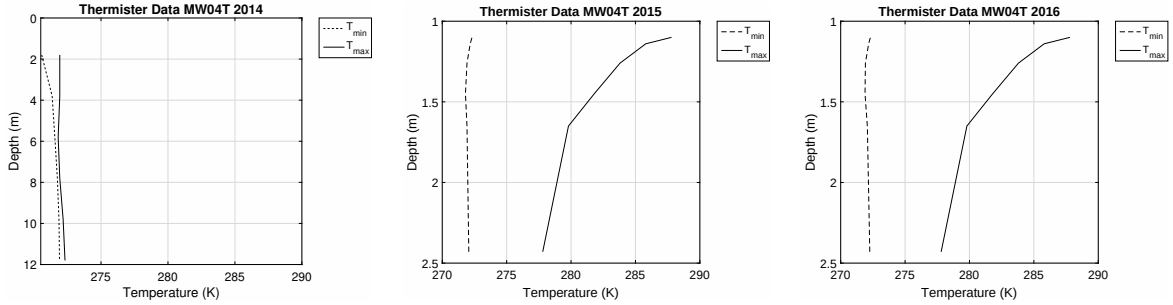

(a) MW04T - 2014 (b) MW04T - 2015 (c) MW04T - 2016

Figure 3.3: Thermister data collected at the MW04T experimental site from 2014, 2015, 2016. Temperature is reported in degrees Kelvin.

3.5.1 Landscape Alterations

The Sahtu Region has been investigated for oil resource exploration, mainly by Imperial Oil, as part of the Canol Project initiative from the mid 1940's. Currently, Husky Energy has explored and is decommissioning this site. Seismic lines and deforestation should be noted as alterations to the natural landscape. Moreover, the region is subject to seasonal wildfires. A major access road has been constructed extending from northeast to southwest from the Mackenzie river for 19 kilometres. The road was constructed using extracted shale and efforts were made to not construct on wetland areas. Other winter access roads were constructed by clear cutting. Old seismic lines and non-developed winter access roads are naturally recovering.

Chapter 4

Methods

4.1 Groundborne Data

Groundborne measurements will be made using geophysical and non-geophysical instruments to estimate where the top of the permafrost is, and where the permafrost thaw occurs relative to land surface features such as tree lines and lake shores. The groundborne data will be collected using the following equipment.

- **Permafrost Probe**: This is a steel rod with a cross handlebar. The probe has measurement marks on the shaft. The device is pushed into the ground until a point where it can not penetrate further, indicating fully frozen water in the matrix. The permafrost depth measurements are recorded by the user.

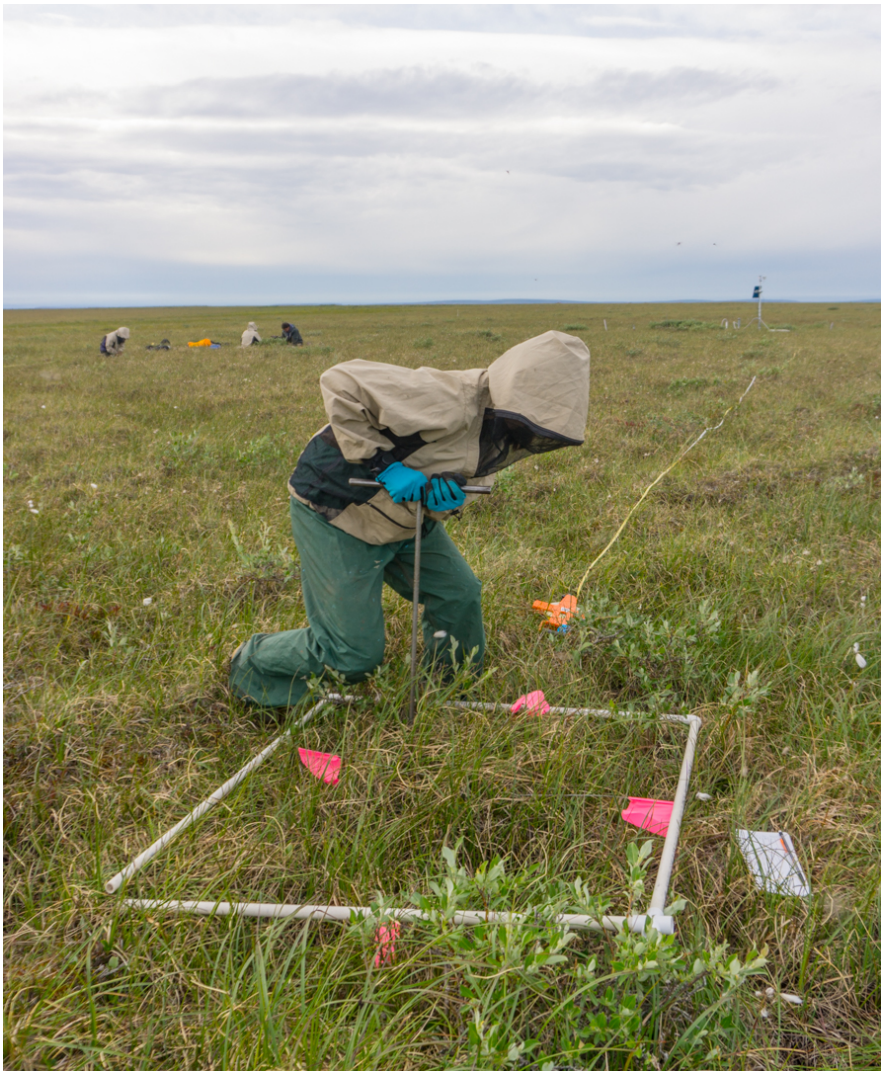

Figure 4.1: Image of a field technician pressing a permafrost probe into the soil. (Hewitt 2017

- **Geonics EM-31**: A frequency domain electromagnetic ground conductivity meter (GCM). The depth of investigation of this system is approximately 1.5 meters below ground surface when held 1 meter above the ground surface in normal walking operations. The device uses a single set of 3.4 meter fixed-separation transmitter and receiver coils. The apparent conductivity measurements displayed by the GCM were recorded by hand.

Figure 4.2: Geonics EM-31 Ground Conductivity Meter system. (Magna Enterprises Undated

- **Geonics EM-34**: This is also a frequency domain electromagnetic GCM, which uses two coils with variable separation capabilities. The system can be configured to operate at 10 meter, 20 meter, or 40 meter coil separation, which provides depths of investigation of 15, 30 and 60 meters respectively. Data can be logged using a data logger, or if the survey uses the three coil separations, the apparent conductivity measurements displayed by the GCM were recorded by hand by the user. This system requires two people, one to man the transmitter coil, and the other to man the receiver coil. The separation is made manually and since both coils are independent of one another, the two operators will have to pay attention to proper coil position and orientation, otherwise, measurements will be inaccurate.

Figure 4.3: Geonics EM-34 Ground Conductivity Meter system. (Geomatrix LTD Undated

- **Syscal Junior 48**: The ERT system is equipped with 48 electrodes and one switch box. The switch box includes a data storage unit and can produce ERT surveys using various spatial configurations of the electrodes. The electrodes are 6 inches long, and are driven into the ground by hand or by mallet. The electrodes are connected together by a shielded cable with exposed wire at five meter intervals. The switch box includes a computer and data recorder. The system's computer records resistivity measurements, and are subsequently downloaded to a computer and displayed using proprietary software from Iris Instruments.

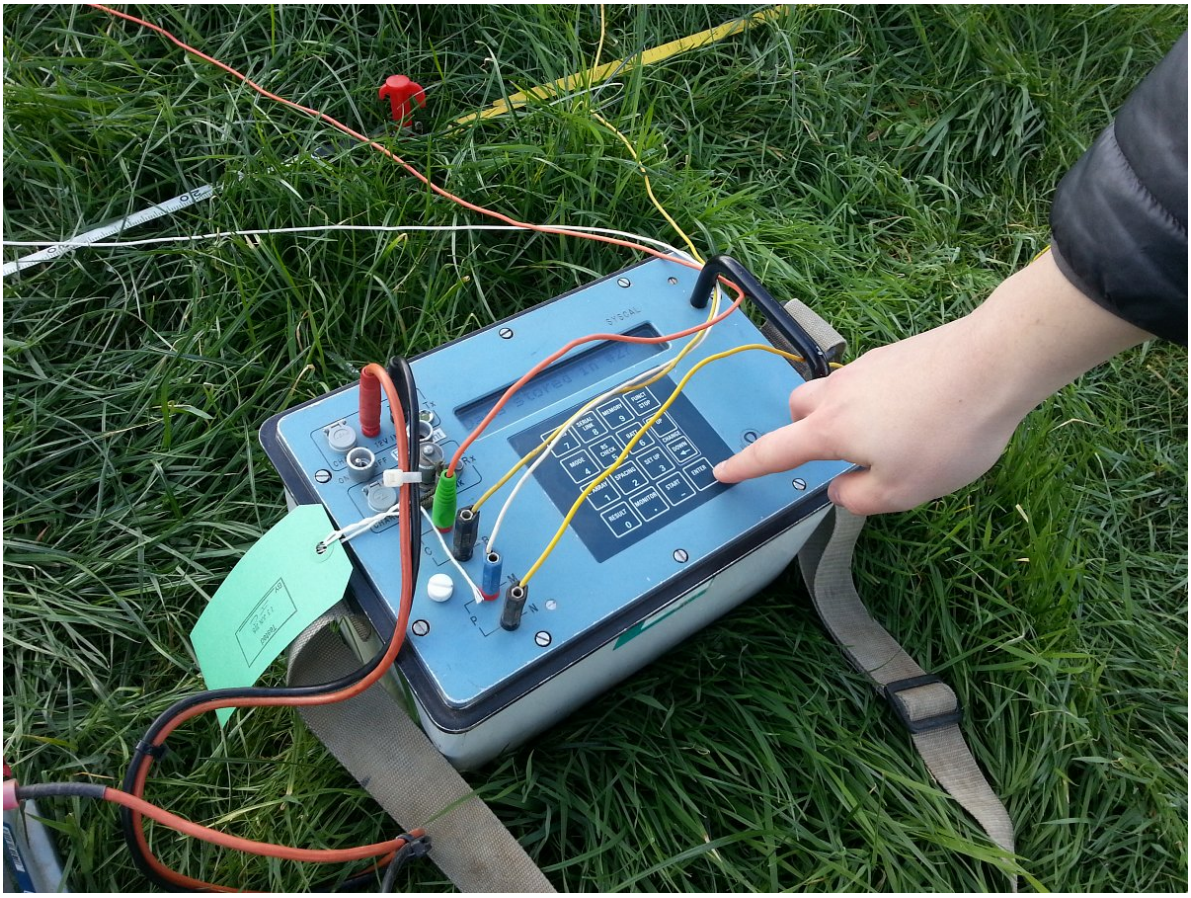

Figure 4.4: Syscal Switch 48 Junior Electrical Resistivity Tomography system. (Geomatrix LTD Data Sheet Undated)

(a) Setting up the ERT system at the MW04T site.

(b) Setting up the EMI (Geonics EM-34) system at the MW04T site.

(c) Setting up the EMI (Geonics EM-34) system at the Marg Lake site.

Figure 4.5: Field site photos with equipment used to perform electrical surveys.

In the following sections, we will describe the theories and specific methodologies relevant to the work on this peoject.

4.2 Theory

The methods presented in this work exploit the concept of apparent ground conductivity σ_a, which is measured and indicated by a ground conductivity meter (GCM) using the following formulation:

$$\sigma_a = 4\frac{\left(\frac{H_S}{H_P}\right)}{\mu_0 \omega s^2} \tag{4.1}$$

where H_P is the primary electromagnetic field generated by the transmitter coil as measured by the receiver coil, H_S is the secondary electromagnetic field measured by the receiver coil, as a result of the interaction of the primary field with a subsurface conductor, μ_0 is the magnetic permeability of free space ($4\pi \times 10^{-7}$ H/m), ω is the angular frequency of the electromagnetic field, and s is the spacing between the transmitter and receiver coils. In most geophysical monitoring techniques, s, ω are controlled and H_S and H_P are observed. The experiment took advantage of the frequency domain electromagnetic (FDEM) method, where an electromagnetic field is generated by a transmitter that has a constant continuous current.

The measurement depth, i.e., the depth at which the apparent ground conductivity is measured, is a function of the coil spacing and orientation of the transmitter and receiver coils. Based on the elliptical nature of the emitted electromagnetic field from the transmitter coil, and the electromagnetic field lines and field flow direction, a vertical dipole has a greater depth of penetration compared to the horizontal dipole coil configuration. Figure 4.7 shows the significant differences in sensitivity patterns between the horizontal and vertical dipole configurations. *Sensitivity* here is the relative effect (or influence) of the soil on the measurement of apparent conductivity, such that a lower sensitivity would have marginal to no influence on the measurement of apparent conductivity. The vertical sensitivity profile shows little to no sensitivity at the ground surface, and is highly sensitive to the presence of a subsurface body at a measurement depth determined by the electromagnetic field strength and coil separation. The horizontal sensitivity profile exaggerates the surface and near-surface features. There is a significant level of sensitivity at a similar depth of investigation in the vertical dipole configuration, however those electromagnetic interactions are subdued by the vastly higher sensitivity of the near-surface interactions. The sensitivity profiles are characterized by using the two sensitivity functions, equations 4.2 and 4.3, for each of the coil configurations. It is important to note that depth z is normalized by dividing the true depth by the coil spacing.

$$\phi_V(z) = \frac{4z}{(4z^2 + 1)^{3/2}} \tag{4.2}$$

$$\phi_H(z) = 2 - \frac{4z}{(4z^2 + 1)^{1/2}} \tag{4.3}$$

The peak sensitivity of the GCM is reliant on these formulations, and are outlined in the technical documents from the manufacturer of the equipment used. Table 4.1 lists

the various equipment used for the EMI surveys as part of this work, and their respective investigation depths.

Table 4.1: Peak sensitivity depths for both horizontal and vertical dipole configurations at multiple coil separation. The equipment used are the EM-31 and EM-34. The $+h$ indicates that the equipment was held one meter above the ground surface.

Equipment	Coil Spacing s (m)	Peak $^{H}\|\phi$ depth z (m)	Peak $^{V}\|\phi$ depth z (m)
EM-31	3.4	2.55	5.1
EM-31+h	3.4	1.55	4.1
EM-34	10	7.5	15
EM-34	20	15	30
EM-34	40	30	60

Given the nature of the primary magnetic field, and its interactions with the subsurface, the conductivity measurement is subject to an averaging of the conductivity within a sampling volume which is proportional to the spacing between the transmitter and receiver coils.

The dipole-dipole configuration was used for the ERT surveys. The geometry allowed for a higher electrical flux through the resistive permafrost zone. The mathematical formulation to determine the potential difference between the dipoles is:

******* ADD PICTURE OF DIPOLE DIPOLE ERT *******

$$\Delta\Phi = \frac{I\rho}{2\pi}\left\{\frac{1}{C_1P_1} - \frac{1}{C_1P_2} - \frac{1}{C_2P_1} + \frac{1}{C_2P_2}\right\} \tag{4.4}$$

where ρ is the resistivity, C_x and P_x are the positions of the current and potential electrode respectively, and I is the current though the current electrodes. The formula defining the potential difference can be rearranged and associated to a geometric factor G. Therefore we get the following formula for apparent resistivity (ρ_a):

$$\rho_a = G\frac{\Delta\Phi}{I} \tag{4.5}$$

The dipole-dipole configuration has a geometric factor of:

$$G = \pi n(n+1)(n+2)a \tag{4.6}$$

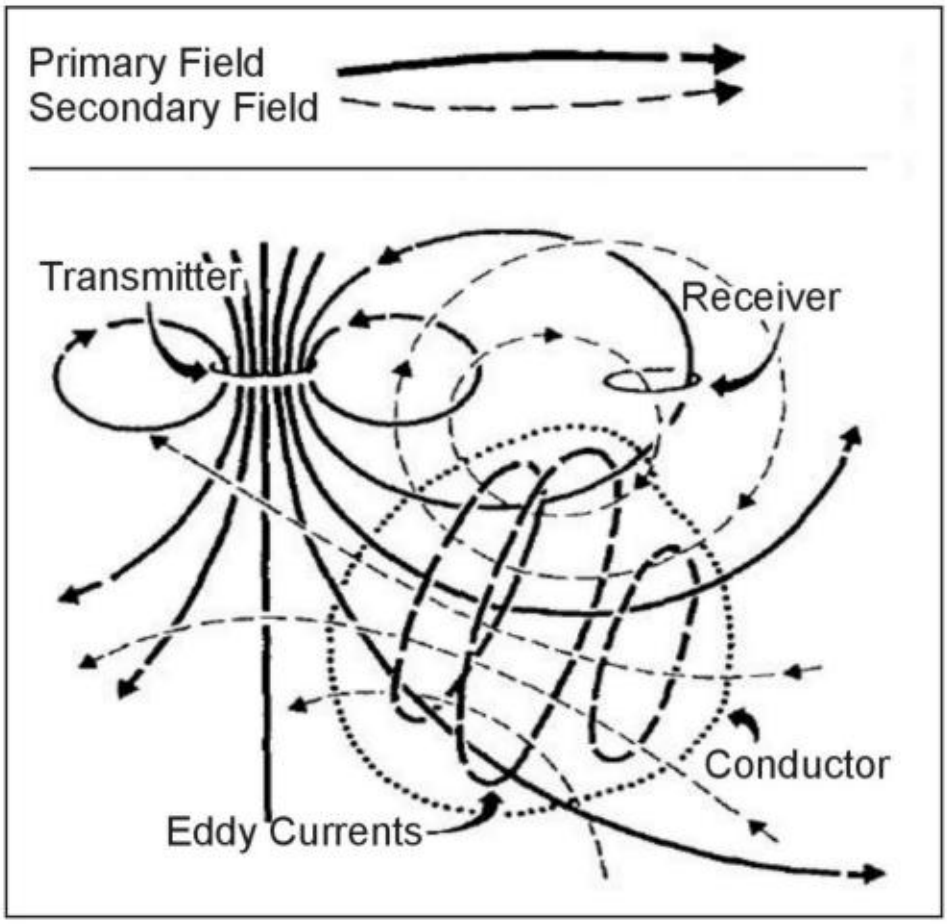

Figure 4.6: Schematic representation of electromagnetic induction in geophysics. (Wightman et al 2003)

where a is the separation between electrodes, and n is the integer multiplier index to the spacing variable a. Substituting Equation 4.6 into Equation 4.5, we get:

$$\rho_a = \pi n(n+1)(n+2)a\frac{\Delta\Phi}{I} \tag{4.7}$$

The dipole-dipole electrode configuration yields in theory the highest electrical current density in the ground. This is advantageous due to the resistive nature of the permafrost.

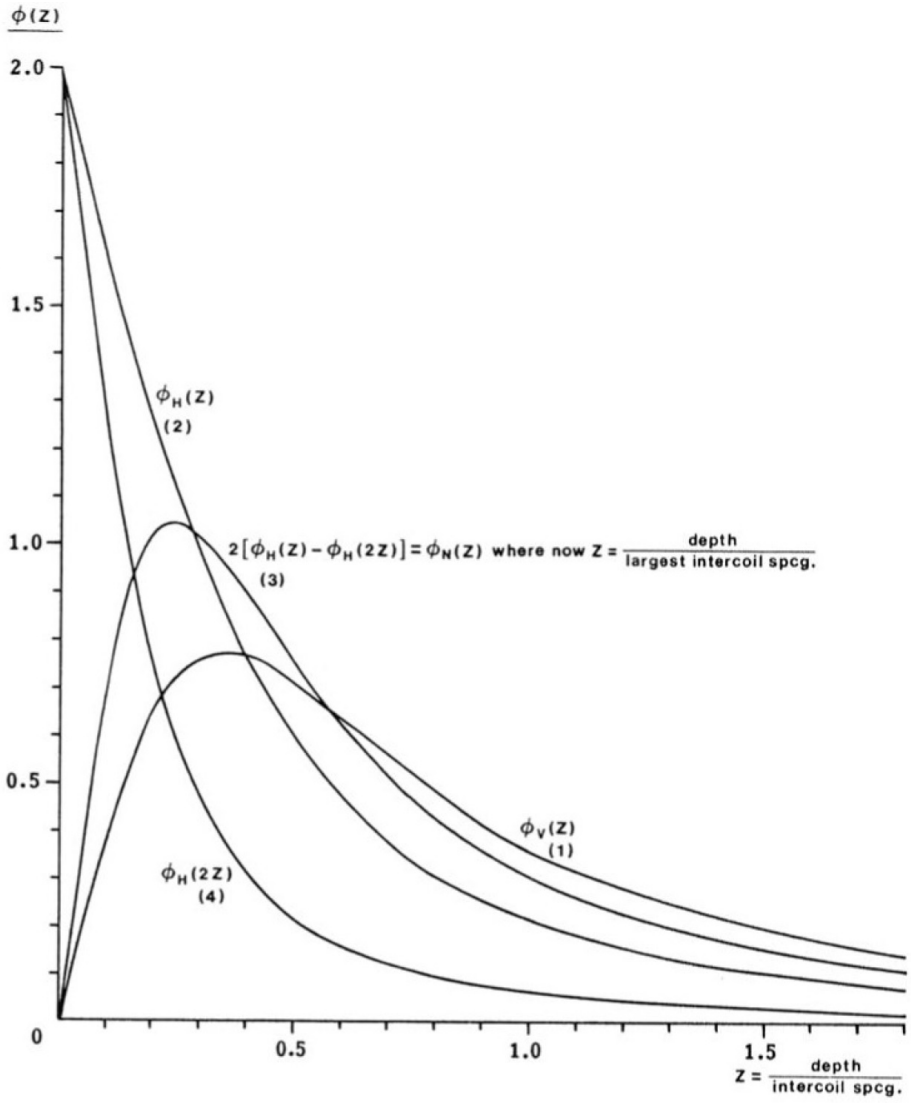

Figure 4.7: Sensitivity profile of the Geonics EM-34-3^{TM} frequency domain GCM. (TN6-Geonics, McNeil 1980)

4.3 Hypothesis

4.3.1 Electrical Methods

The problem statement relies on the principle of electrical resistivity. The first presumption is that water in its solid phase as ice is significantly more resistive than water in its liquid phase, it is assumed that the water is not pure and has dissolved solids from the surrounding geology, making it conductive.

4.3.2 Ground Decoupling

The two electrical methods (ERT and EMI) used in this experiment yield potentially similar results and, depending on geologic situation, interpretation. They differ however on the basis of principle. The ERT system requires ground coupling of the equipment, this is in the form of electrodes that penetrate in the ground. Electrical coupling must be established between the electrode and the soil it is inserted into. In contrast to this method, a GCM can use the principle of electromagnetic induction (EMI) whereby an electromagnetic field is generated and requires no ground coupling. The system can be operated at ground surface or suspended in the air. It is estimated that the GCM will interact with the ice and water in similar fashion as the ERT system. The conductivity measured by the GCM and ERT will be higher than that of ice.

4.3.3 Vertical Sounding

We expect that this experiment will produce vertical conductivity variation of the permafrost rich area proportional to the coil separation. We subsequently presume that these measurements will provide information about the subsurface similar to the ERT measurements.

4.3.4 Convergence

Based on the vertical measurements made by the GCM, we speculate that there will be convergence of electromagnetic measurements as the permafrost table deepens, since the shallower measurements will demonstrate an earlier higher-conductivity response compared to the deeper media, and that when the permafrost table is deep enough, the deeper

measurements will catch up to the shallower results. We estimate that the permafrost will be thawed gradually vertically along a survey line. The change in permafrost table depth, along the survey line, will mean that measurements made at a certain depth will show high resistivity in a shallow permafrost zone, but will manifest an increase in conductivity as the permafrost table progressively deepens and water in liquid phase begins to dominate.

4.4 Location Selection

Site selection and survey line design relied heavily on the nature and magnitude of the features that were noticed at the ground surface. The sites were selected as a result of significant changes in topology along an arbitrary line. In addition, the locations also required having significantly shallow permafrost. The two sites were labelled as "MW04T", and "Marg Lake". Visually, each site had originally variable vegetation, primarily tree cover. Both sites selected as part of this mission exhibited shallow permafrost. This was tested by using a permafrost probe, which is a simple penetrative process whereby a steel rod with a handle is driven into the ground until it is no longer able to penetrate. This process is trivial in nature, however background geologic information is necessary to determine whether the probe detects permafrost or other geology.

4.4.1 MW04T

The first experimental site has been cleared of trees to allow the drilling of a monitoring well. The soil was not disturbed significantly in the process, thus the soil maintains its original integrity. The drill pad is located adjacent to an all-season industrial access road. The edges of the drill pad are heavily vegetated, with Black Spruce dominating the tree canopy. Fallen branches and light surface vegetation is also present. Canopy density however is variable between the North and South edges of the pad. The canopy is less dense, and trees are shorter on the South edge of the drill pad, conversely, the canopy along the North edge is notably taller and denser. We produced two permafrost profiles for this site to understand the gradient of permafrost deterioration from within the vegetated area to the clearing. The geology of this location is an evenly distributed sandy silt. Along Line 001, we noticed a three meter patch of sand at position 0m.

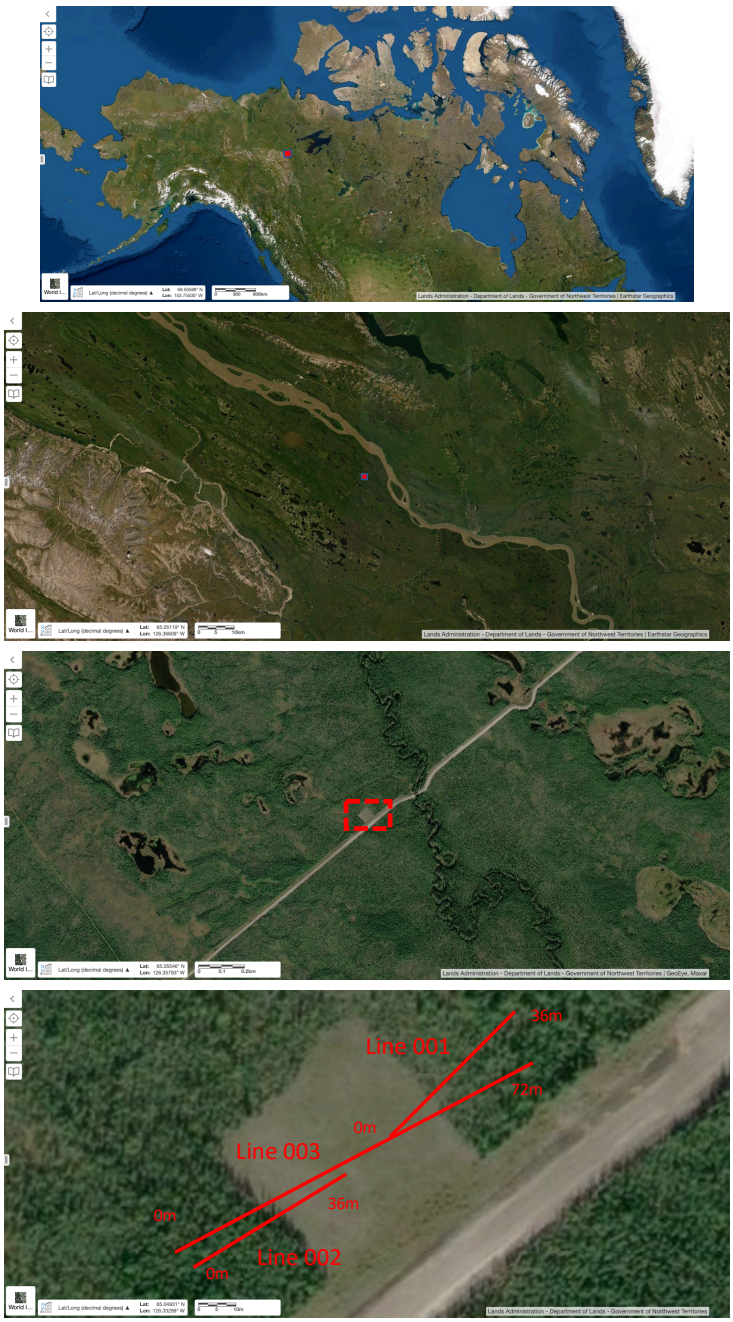

Figure 4.8: Survey location MW04T in the Sahtu Region, of the Northwest Territories, in northern Canada.

4.4.2 Marg Lake

The Marg Lake site is located near the all-season industrial access road however is not in an area of anthropogenic modification. The survey line is located near a lake; permafrost is often absent adjacent to lake and wetland features, thus a transition was expected. The lake is one within a series of lakes that are characteristically linearly oriented. This site was selected due to its medium to dense canopy, however the surface vegetation in this area differs from the MW04T experimental site whereby dense moss is distributed widely. Testing using the permafrost probe indicated very shallow permafrost at the site. The soil horizons is presumed to be horizontally layered in nature at this location. The layers are assumed to be homogeneous, however, we presume clay to be present at around 1 meter depth given the difficulty in penetrating the soil with the permafrost probe nearer to the lake where the permafrost degrades. The soil felt significantly compacted but not impenetrable, leading to believe that permafrost was not hindering the penetration of the probe.

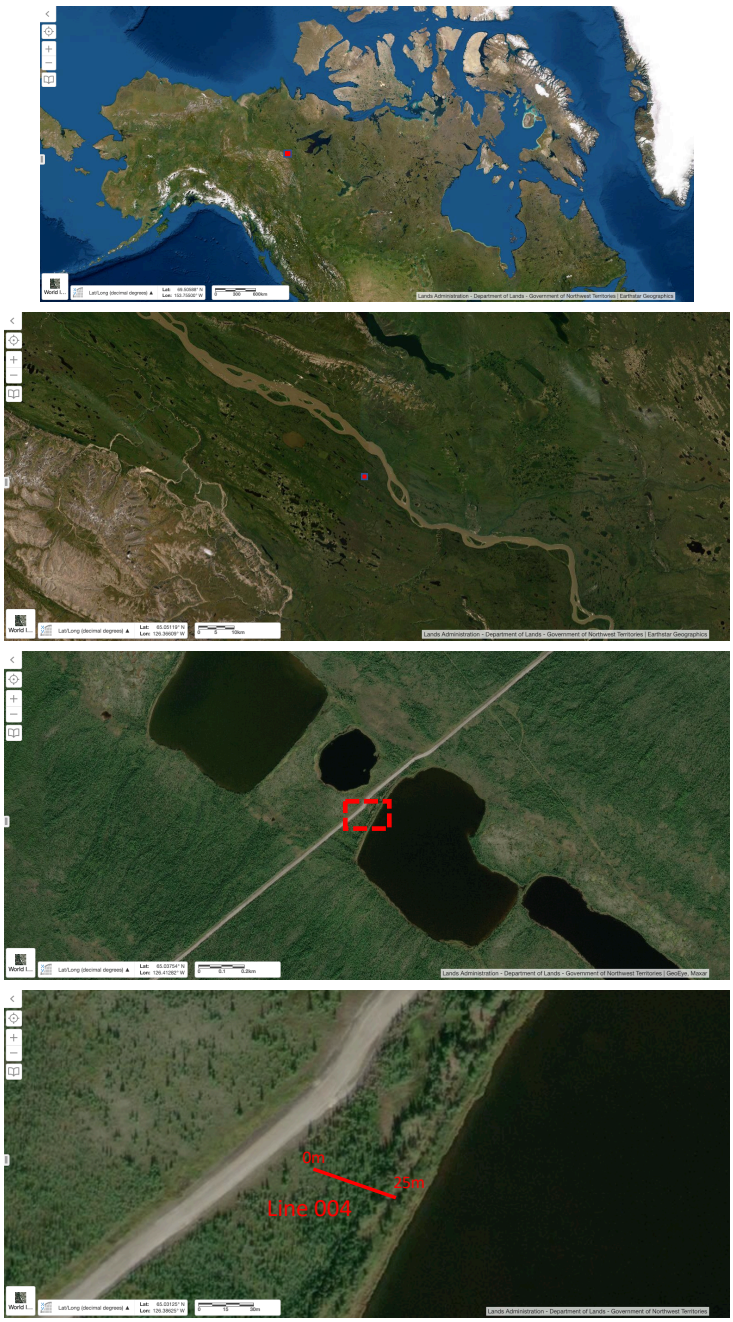

Figure 4.9: Survey location Marg Lake in the Sahtu Region, of the Northwest Territories, in northern Canada.

4.5 Observations

4.5.1 MW04T

Three survey lines were prepared at the MW04T site. Line 001 is positioned on the Southern edge of the drill pad. The survey line is 36 meters in length, beginning 10 meters into the drill pad, with 26 meters within the tree covered area. Line 002 is positioned at the Northern edge of the drill pad. The survey line is 36 meters in length, with 18 meters into the drill pad, and 18 meters within the tree covered area. Line 003 is 72 meters in length and cuts through the drill pad with some of the line in the tree covered areas at both the North and South edges of the drill pad. The ERT system has 48 electrodes, for lines 001 and 002, the electrode spacing was 0.75 meters, for line 003, the electrode spacing was 1.5 meters.

4.5.2 Marg Lake

One survey line was prepared at the Marg Lake site. Line 004 is positioned parallel to the series of lakes, and was 24 meters in length. The ERT electrode separation is 0.5 meters, this is to account for the very shallow nature of the permafrost at this site, similar to the MW04T site.

4.5.3 Inversion

The inversion of the ERT data was done using the GeoTomo Res2DInv^{TM} software package. Parameters were selected to allow the model to produce suitable estimations of resistivity, however the main goal of the inversion modeling is to estimate the depth to permafrost, and the vertical variation of the permafrost table. The following is the configuration of the software for the inverse model:

4.6 Assumptions

There is limited thermistor data from the MW04T experiment site, we assume a horizontally consistent temperature profile through the drill pad around the MW04T monitoring well, furthermore, we assume that the geology is homogeneous and isotropic (within each layer), horizontally layered at all survey sites.

Table 4.2: Method and parameters of each survey line.

Line Number	Method Parameters Site	ERT	EMI
001	MW04T	Electrode spacing = 0.75 m	Horizontal Dipole 20m Vertical Dipole 20m Horizontal Dipole 10m Vertical Dipole 10m Vertical Dipole 3.4m
002	MW04T	Electrode spacing = 0.75 m	Vertical Dipole 10 m
003	MW04T	Electrode spacing = 1.50 m	Horizontal Dipole 20m Vertical Dipole 20m
004	Marg Lake	Electrode spacing = 0.5 m	Horizontal Dipole 10m Vertical Dipole 10m Vertical Dipole 3.4m Horizontal Dipole 3.4m Vertical Dipole 3.4m+h Horizontal Dipole 3.4m+h

Chapter 5

Results

5.1 Introduction

A proof of concept experiment was conducted in August 2018 in the Shatu Region of the Northwest Territories. The field work consisted of using an electrical resistivity tomography (ERT) and electromagnetic induction (EMI) methods. The surveys were conducted in the latter part of the Summer season to take advantage of the potential maximum melt of the subsurface permafrost. There were two locations selected. The sites were selected to understand the electrical signature of the near-surface in regions with landscape variability, and significant hydrologic features, such as streams, rivers, and lakes. The two geophysical methods were used on the same survey lines with less than 24-hour temporal separation to ensure accurate measurements. The equipment used were the Iris^{TM} Syscal 48 Junior, and the Geonics^{TM} EM-34 and EM-31. Survey lines were selected based on their location and the amount of surficial modification, whether it be natural or anthropogenic. A permafrost probe was used to sound the shallow permafrost along our survey lines, and both ERT and EMI methods yielded correlative results.

5.2 Data

Permafrost in the soil of both field sites is ice rich and acts as a resistor because water in solid phase inhibit the movement of free ions in the soil. This is in stark contrast to water in its liquid phase, presumably rich in dissolved solids, which is highly conductive.

5.2.1 Permafrost Probe Data

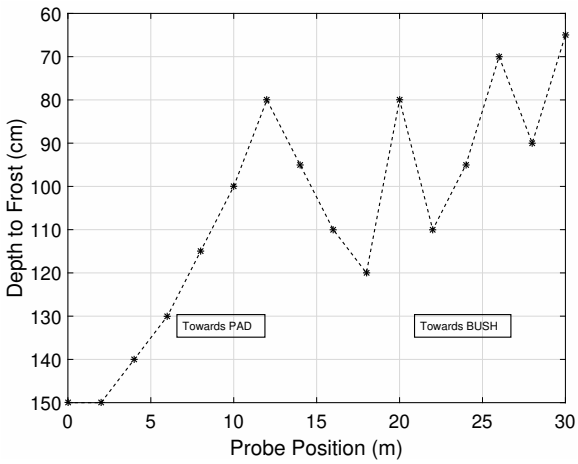

(a) Line 001: Permafrost profile of the Southern edge of the MW04T experiment site.

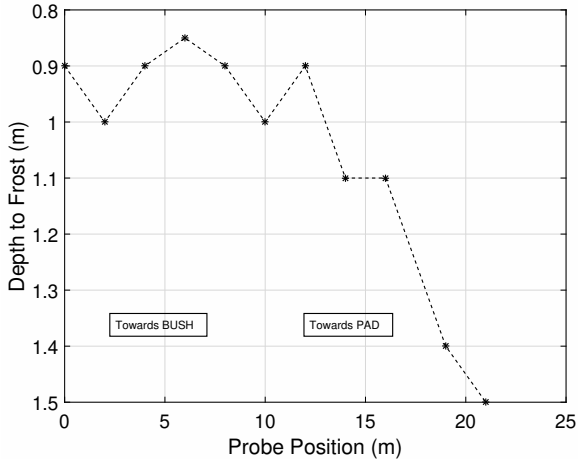

(b) Line 002: Permafrost profile of the Northern edge of the MW04T experiment site

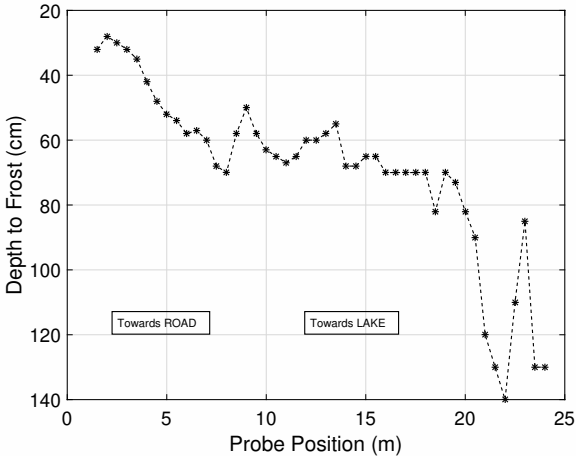

(c) Line 004: Permafrost profile of the Marg Lake experiment site

Figure 5.1: Permafrost probe measurements from both MW04T.

The first dataset collected was permafrost probe measurements. The probe measurements indicated very shallow permafrost on lines 001, 002, and 004. Permafrost table depth plunged at the drill pad boundaries at MW04T, and approximately 10 meters in-land from the shore line at the Marg Lake site. Measurements on Line 001 show a permafrost table

depth of approximately 1.0 meter in the wooded area, however, there is a highly variable zigzag pattern at the surface. We associate this pattern to potential measurement aliasing as a result of low measurement resolution. The zigzag pattern variates the permafrost probe measurements by approximately 0.2 meters. The permafrost table on Line 002 within the wooded area is more consistent, and is estimated around 0.8 to 0.9 meters below the ground surface. The permafrost table plunges more rapidly on Line 002 compared to Line 001. Line 003 was not surveyed using the permafrost probe, since the permafrost table was too deep. Line 004 at the Marg Lake had very shallow permafrost, at an estimated 0.4 meters in the thicker wooded area, then dropping to approximately 0.7 meters in the lightly wooded area, and finally plunging around the 20 meter survey position.

5.2.2 Electromagnetic Induction Data

MW04T - Line 001 EMI

The measurements made along survey Line 001, depicted in Figure **??** show an increasing trend in conductivity from within the heavily vegetated area towards the drill pad. The measurements of the VD20m, HD20m, VD10m, and HD10m converge from within the vegetated area towards the drill pad. However, the VD3.4m diverges from the other measurements. The divergence could be symptomatic of a thawed-out near-surface with high moisture content whereas deeper could still be significantly frozen. The line has two slopes for VD3.4m, the switch occurs at the 10 meter position, where the permafrost table depth increases significantly, as seen in Figure **??**. It is important to note that VD20m exhibits irregular behaviour within the vegetated area. The measurements are steadily and markedly high then suddenly drops to converge with the other measurements. This drop occurs at the same location where the slope of the line switch in VD3.4m.

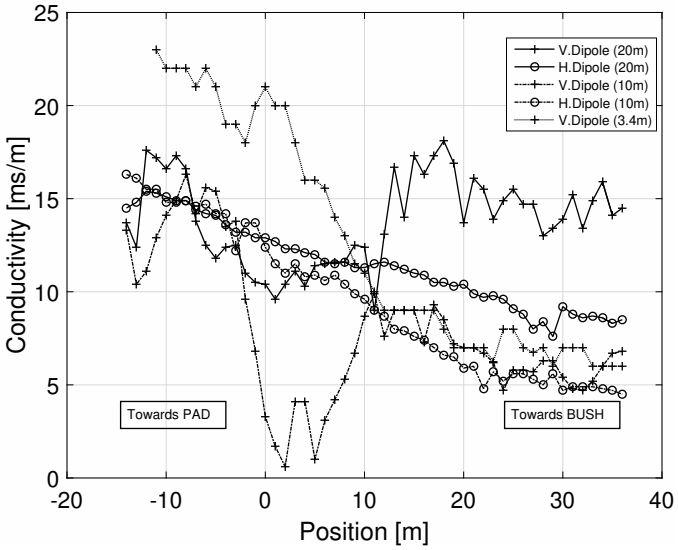

Figure 5.2: Electromagnetic Induction profile of *Line 001*

MW04T - Line 002 EMI

There is an increasing trend in the conductivity measurements collected from within the vegetated area towards the drill pad. The positive trend is linear in nature. From position 0m to 10m, the conductivity remains fairly constant. Upon breaking through the vegetation boundary located at the 12 meter position, the conductivity begins a steady increase.

MW04T - Line 003 EMI

There was no EMI survey conducted on Line 003.

Marg Lake - Line 004 EMI

The data collected at this site involved raising and lowering the EM-31 system (3.4m coil separation) from the ground surface to approximately 1 meter above the ground surface (denoted as +h). The measurements are similar when the sensor is on the ground and when it is elevated. HD3.4m and HD3.4m+h exhibit the lowest conductivity measurements, steadily constant at or about 5mS/m, whereas the VD3.4m and VD3.4m+h are marginally higher at or about 10mS/m. The measurements of HD10m are very close to

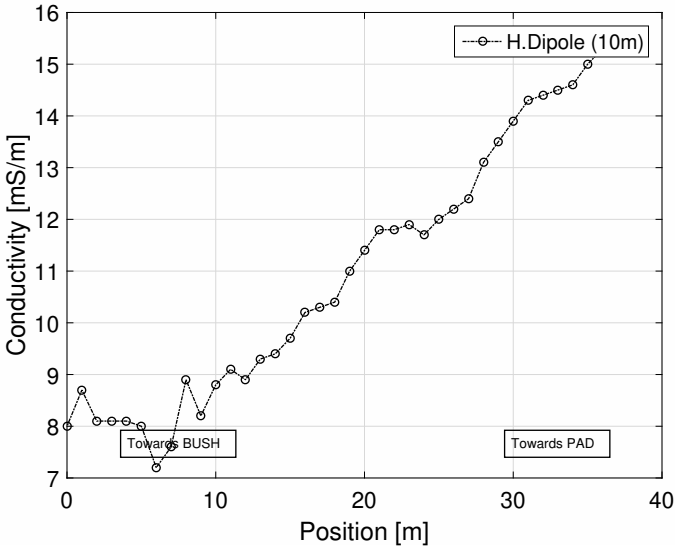

Figure 5.3: Electromagnetic Induction profile of *Line 002*

the VD3.4m and VD3.4m+h measurements and rises slightly more steadily than the EM-31 measurements.

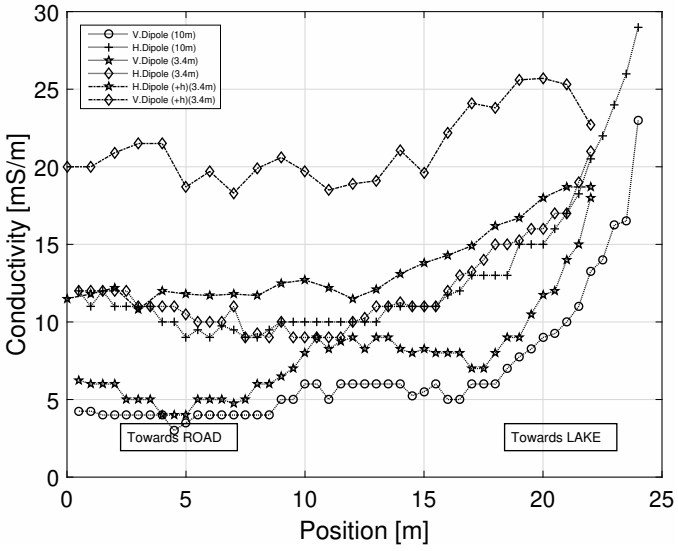

Figure 5.4: Electromagnetic Induction profile of *Line 004*

5.2.3 Electrical Resistivity Tomography Data

The resistivity profile on Line 001, depicted in Figure 5.22a demonstrates a large amount of high resistivity measurements. The calculated resistivities as a result of the inversion are on the order of 400 Ωm to above 1667Ωm. The abrupt transition from higher to lower resistivity occurs at a depth of approximately 0.9 meters. The transition features irregularities such as round peaks and troughs. The resistivity plateau dives at approximately the 7 meter position.

Similar to Line 001, Line 002 also demonstrates a significant presence of high resistivity material within the pseudosection. The higher resistivity region is calculated by the inversion as approximately 700 Ωm to above 1536 Ωm. The high resistivity region shows a regular transition at at a depth of approximately 0.9 meters below the ground surface. The resistivity transition sharply drops in elevation at approximately the 19 meter position.

The resistivity profile of Line 003 shows a sunken high resistivity zone. Resistivities are lower in general compared to lines 001, 002, and 004. The high resistivity zone is calculated by the inversion on the order of 140 Ωm to above 377 Ωm. Nonetheless, there is an evidently tight gradient between the high and low resistivity zones. The high resistivity zone rises slightly near both ends of the pseudosection. The depth of the high resistivity plateau is approximately 5 meters, and is slightly irregular. There is a higher resistivity mound near the 17 meter position.

The resistivity profile of Line 004 demonstrates a very high resistivity region that is predominantly above 3000 Ωm. The high resistivity zone transitions at approximately 0.5 meters, and does not show much irregularities. The transition sharply drops in elevation at approximately at the 17 meter position.

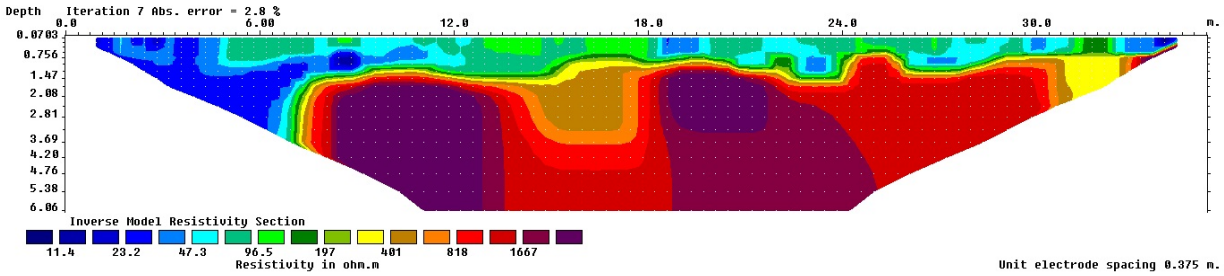

(a) MW04T - Line 1 ERT Pseudosection.

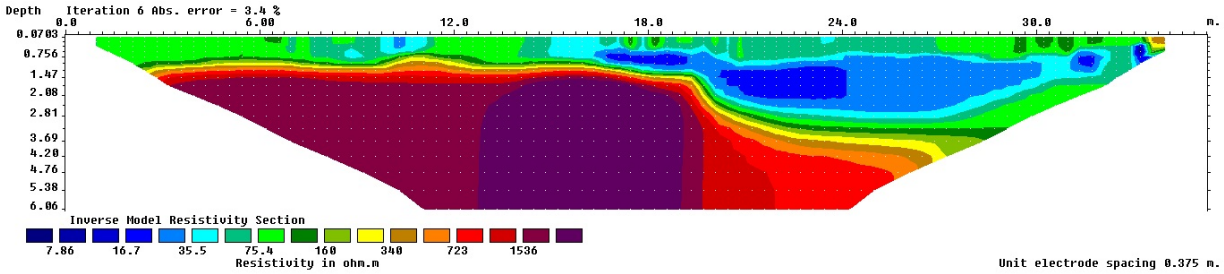

(b) MW04T - Line 2 ERT Pseudosection.

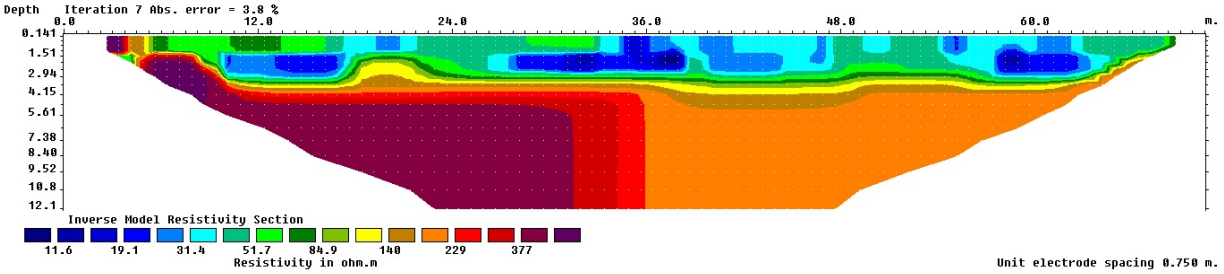

(c) MW04T - Line 3 ERT Pseudosection.

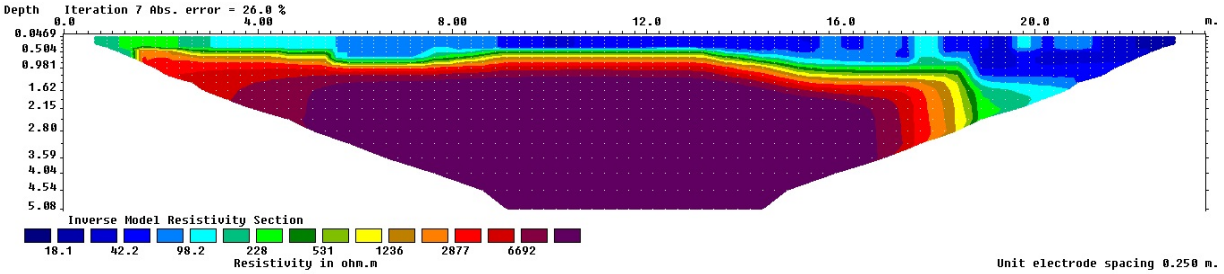

(d) Marg Lake - Line 4 ERT Pseudosection.

Figure 5.5: ERT pseudosections of all four survey lines.

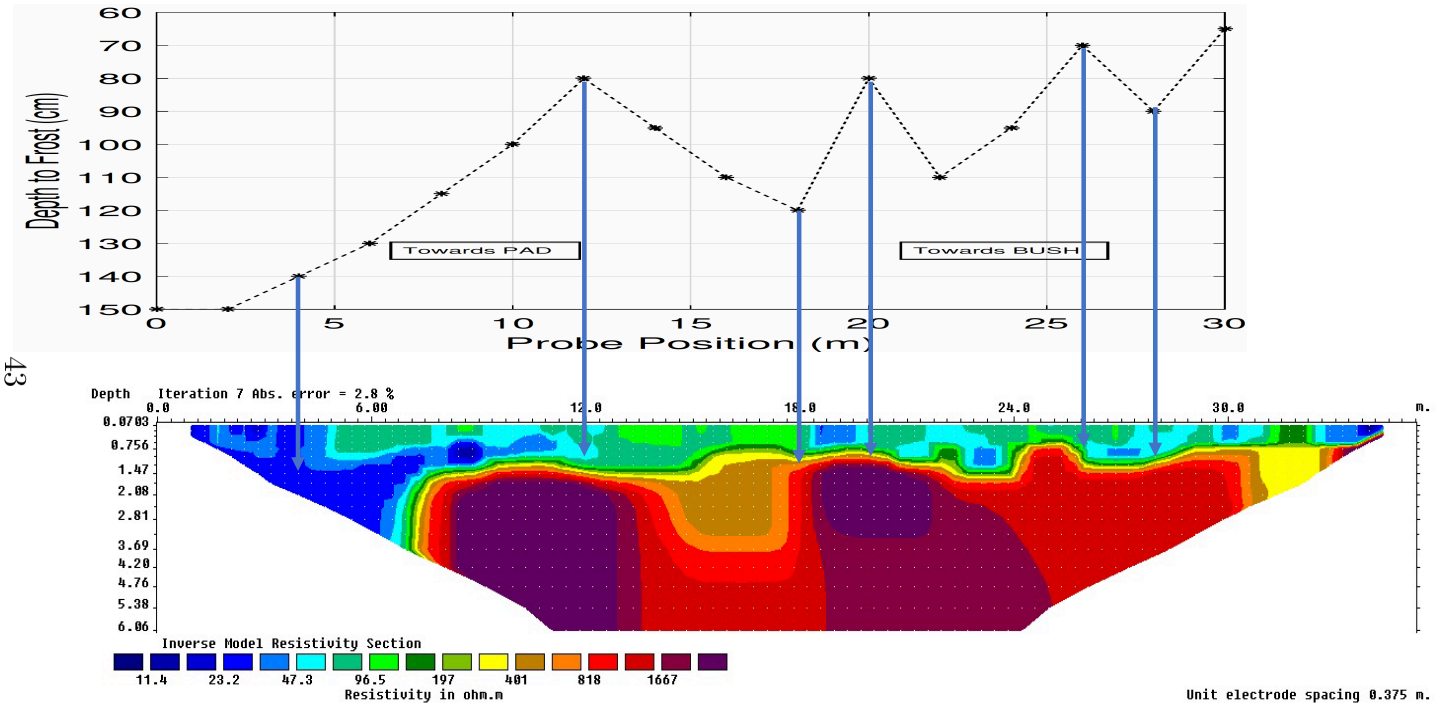

MW04T - Line 1 ERT Pseudosection.

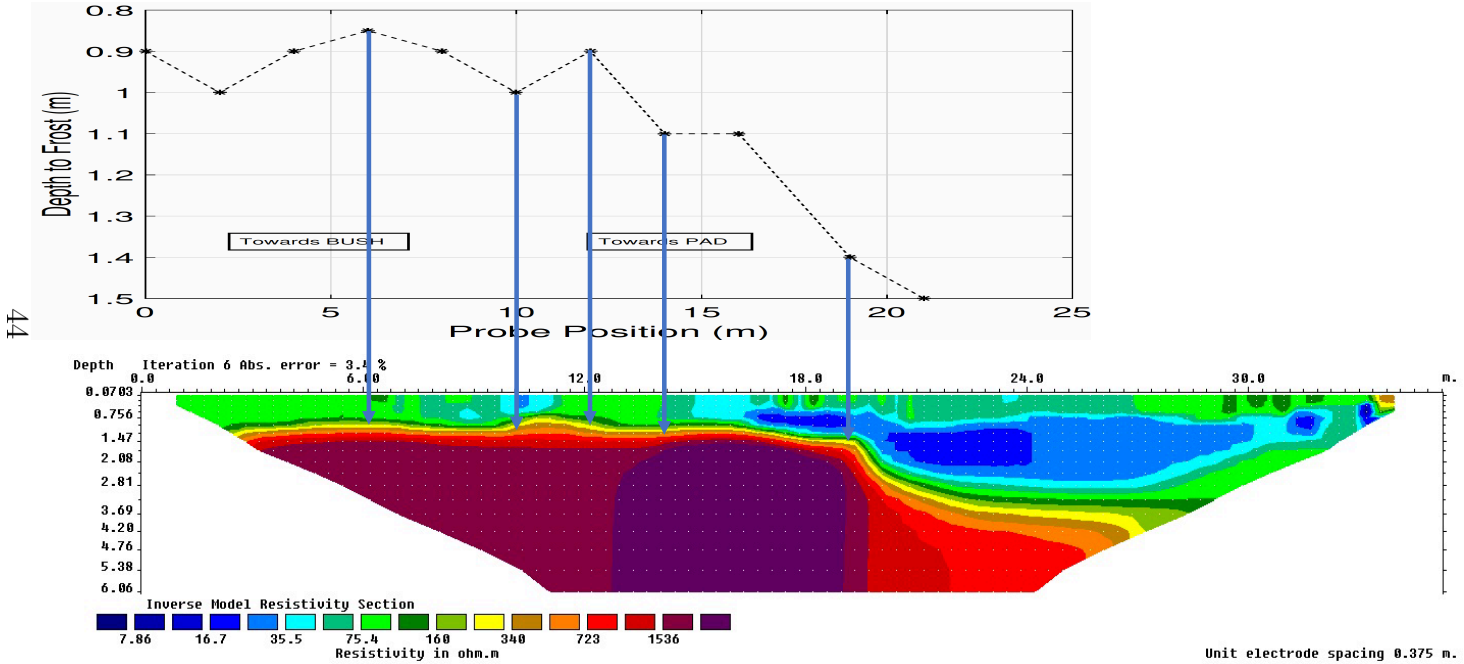

MW04T - Line 2 ERT Pseudosection.

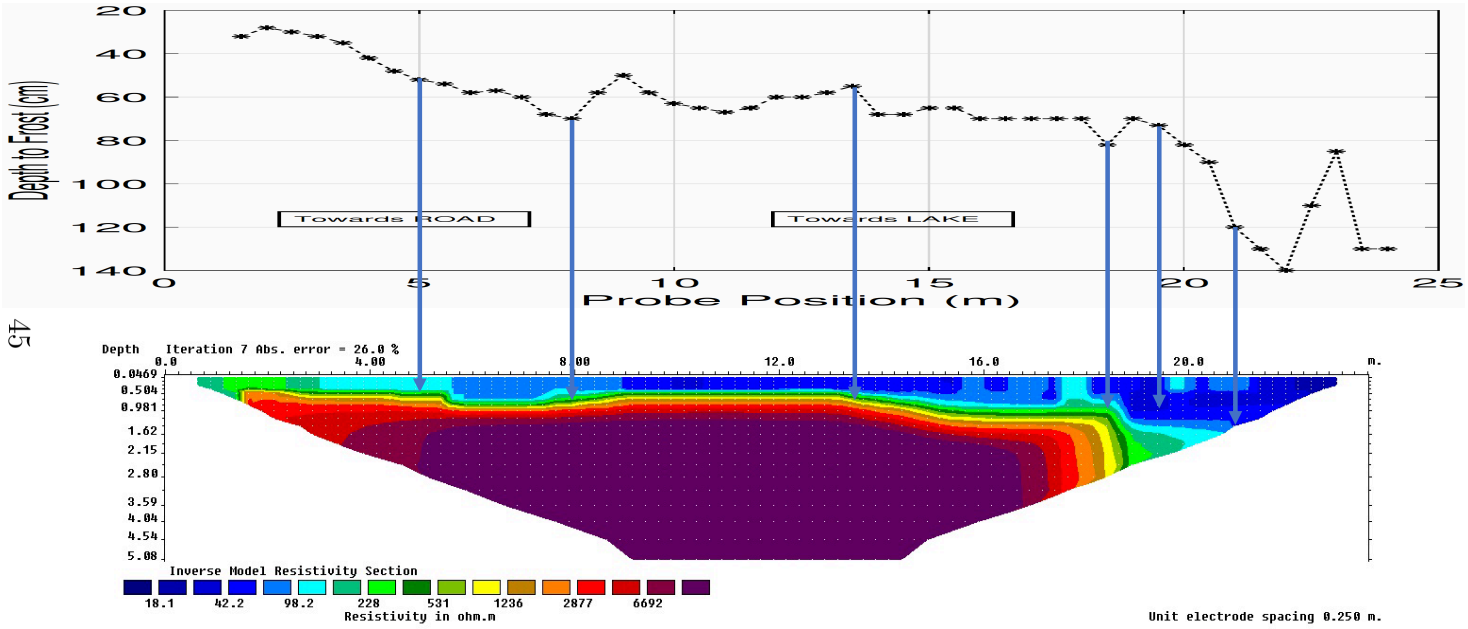

Marg Lake - Line 4 ERT Pseudosection.

5.3 Interpretation

The three principle survey lines for this mission all show similar trends in the measurements. The interaction of the electromagnetic field generated by the GCM, and the subsequent results abide by the presumption that ice acts as a resistor in the general electrical regime of the survey area, and that conversely, the water is a conductive anomaly.

5.3.1 Interpretation of ERT Pseudosections

Line 001

The inverted resistivity data clearly resolves the zone where we estimate the permafrost table to be present in agreement with the permafrost sounding data using the permafrost probe. We note that the gradual nature of the plunging permafrost table in correlation with the thinning of the canopy is exhibited in the inverted data. The pattern in the pseudosection also agree with the electromagnetic measurements along this line. Between the 13 meter and 18 meter position, there is a small less resistive feature manifesting a significant contrast to the surrounding more resistive zone below the anticipated permafrost table. A similar feature is present at the 32 meter position. The inferred permafrost table rapidly plunges at the 8 meter position, concurrent with our hypothesis that the presence of the drill pad has caused depletion of the permafrost in this region, likely due to increased energy at the ground surface due to lack of vegetation cover.

Line 002

Resistivity measurements made along this line appear to show a clear and sharp decline in the permafrost table towards the drill pad. The resistive zone is more constant and persistent throughout in the vegetated zone without many contrasting features. The permafrost table plunges near the boundary of the vegetated zone and the drill pad at the 19 meter position, the plunge is halted at a depth of approximately 2.5 meters. This was undetectable using the permafrost probe since it was too deep.

Line 004

The pseudosection shows a uniform depth of the resistivity discontinuity in electrical resistivity along the survey line until the 18.5 meter position. The resistive zone is very shallow and shows a sharp plunge progressively towards the lake. There is a slight downward gradient in the permafrost table between the 13 meter and 18 meter position. The vegetation was notably thinner in comparison to the vegetation towards the access road. The thinner canopy also had a higher moss content on the ground.

5.3.2 Joint Interpretation of ERT and Permafrost Probe Data

The permafrost probe measurements have been plotted against the visually interpreted depth to permafrost from the ERT pseudosections in figures 5.6,5.7, 5.8.

Line 001

The permafrost probe measurements on Line 001 show a vertically zig-zag style pattern, ultimately showing the plunge of the permafrost table at the edge of the drill-pad. The depth of the permafrost as interpreted from the ERT pseudosection correlates fairly well laterally. The ERT interpretation, however, is vertically stretched positively and negatively compared to the permafrost probe measurements. At the 25 meter position, the ERT inversion detected a slight rise of the permafrost table, though it was not detected in the permafrost probe data. Nevertheless, it is evident that the ERT interpretation clearly shows a plunging trend in the permafrost.

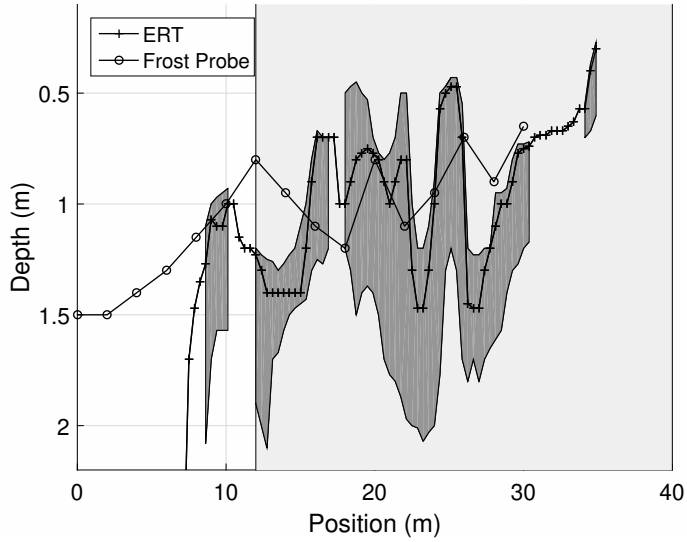

Figure 5.6: ERT permafrost depth estimate against permafrost probe measurements. Line 001. The light-gray shaded area represents the vegetated/forested area. The dark-gray shaded area represents the interpretation's estimated permafrost table depth with uncertainty.

Line 002

The two curves are more correlative in Figure 5.7. Similarly to Line 001, the vertical variation in the permafrost table is identified in both the interpreted permafrost depth, and the permafrost probe measurements. There is a similar trend to Line 001 where the ERT data is vertically stretched, but mainly in the positive direction. The permafrost table plunges almost identically on both curves.

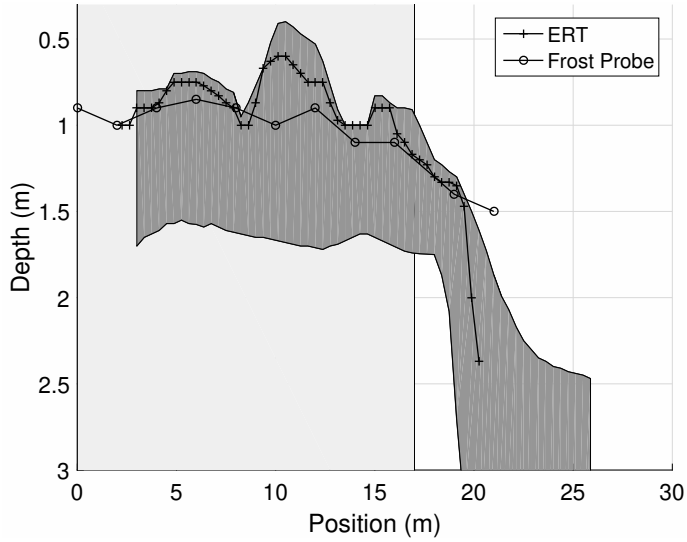

Figure 5.7: ERT permafrost depth estimate against permafrost probe measurements. Line 002. The light-gray shaded area represents the vegetated/forested area. The dark-gray shaded area represents the interpretation's estimated permafrost table depth with uncertainty.

Line 004

Unlike figures 5.6 and 5.7, Line 004 demonstrates vertically correlative data until the approx. 15 meter position, where the interpreted ERT permafrost depth rapidly increases ahead of the permafrost probe measurements. There is a significant lateral disparity between the ERT measurements and the permafrost probe measurements. The permafrost plunges at the 13 meter position on the ERT data, and plunges at the approx. 20 meter position on the permafrost probe curve.

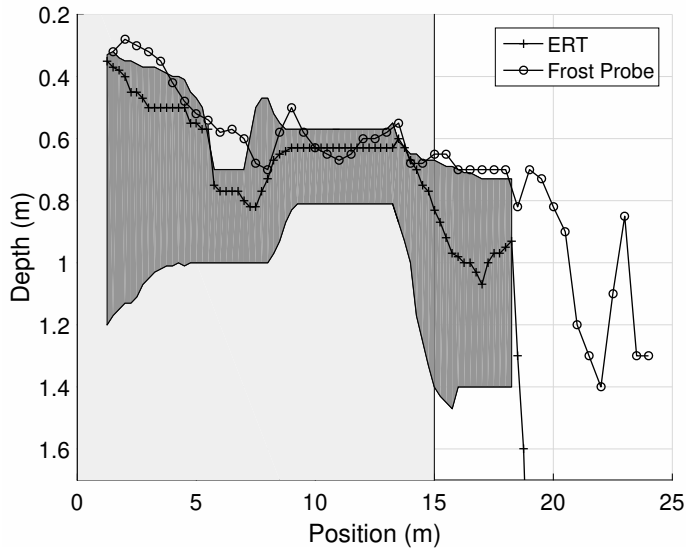

Figure 5.8: ERT permafrost depth estimate against permafrost probe measurements. Line 004. The light-gray shaded area represents the vegetated/forested area. The dark-gray shaded area represents the interpretation's estimated permafrost table depth with uncertainty.

5.3.3 Correlation of EMI and Permafrost Probe Data

Line 001

All electromagnetic measurements show a reliably increasing trend as the permafrost table deepens. Figures 5.9 to 5.13 make it evident that there is variation in the conductivity measurements as a function of coil separation and coil orientation (i.e. vertical versus horizontal dipole).

Line 001 - EM-31 Horizontal Dipole

The EM-31^{TM} has a clearly apparent background conductivity where the permafrost is shallow. The electromagnetic measurements begin a noticeable rise around the 15 meter position. The permafrost probe measurements drop at approximately the 10 meter position.

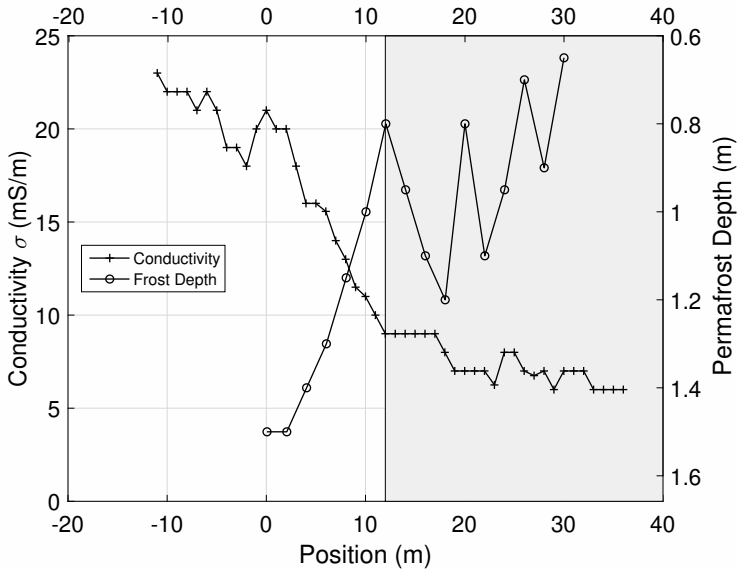

Figure 5.9: Electrical conductivity against permafrost probe measurements. Line 001. Configuration: EM-31, horizontal dipole, 3.4 meter separation. The gray shaded area represents the vegetated/forested area.

Line 001 - EM-34 Horizontal Dipole

The horizontal dipole configuration produced significantly less noisy data compared to the data collected in the vertical configuration. The two coil separations show a similarly increasing slope, and line up fairly well with the plunging permafrost. The lateral disparity between the change in modality of the conductivity curve versus the position where the permafrost table plunges, is caused by the nature of the GCM as it surveys elliptically the entire space between the transmitter and receiver coils. Therefore, as will be evident in the subsequent EMI measurements, the permafrost probe measurements will "lag" behind the EMI measurements.

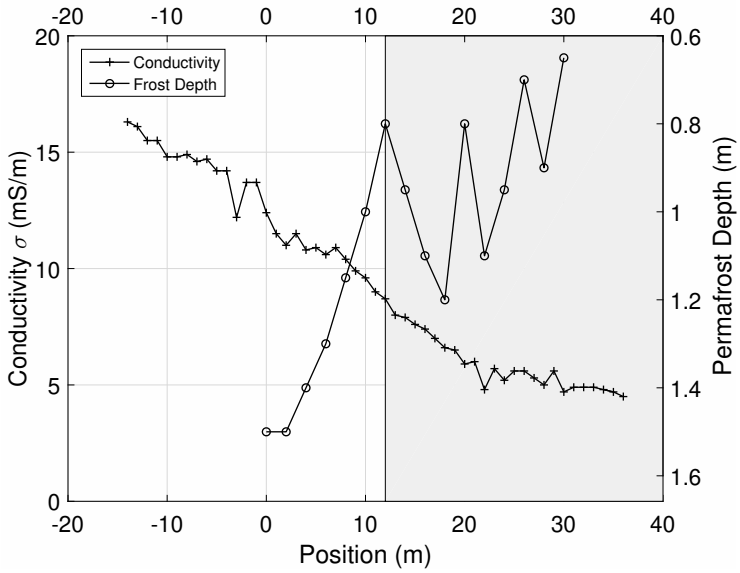

Figure 5.10: Electrical conductivity against permafrost probe measurements. Line 001. Configuration: EM-34, horizontal dipole, 10 meter separation. The gray shaded area represents the vegetated/forested area.

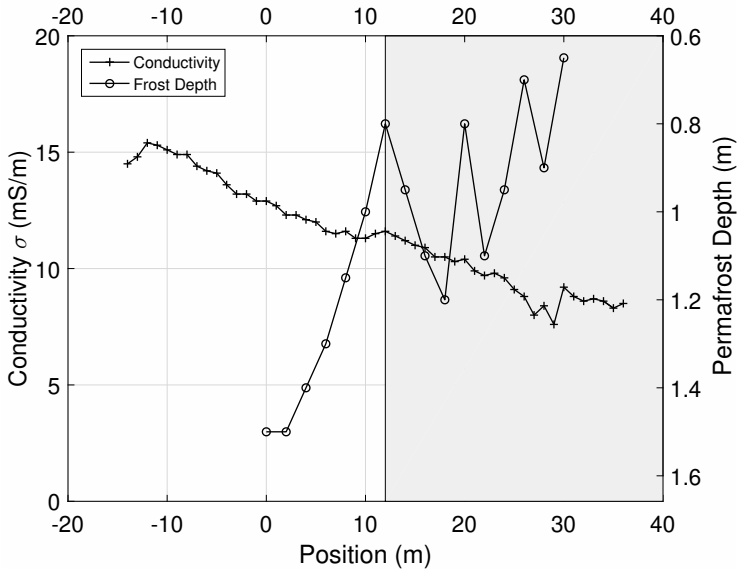

Figure 5.11: Electrical conductivity against permafrost probe measurements. Line 001. Configuration: EM-34, horizontal dipole, 20 meter separation. The gray shaded area represents the vegetated/forested area.

Line 001 - EM-34 Vertical Dipole

The vertical configuration of the EMI survey is much noisier than its horizontal counterpart. Figures 5.12 and 5.13 demonstrate marginal correlation between the electromagnetic data and the permafrost probe measurements. Despite the noisiness of the data, the VD20 results shows a correlation with the permafrost probe measurements compared to the VD10 results. Furthermore, it is important to note that the electromagnetic conductivity rises as the permafrost plunges. The electromagnetic data within the wooded area is not very reliable as the readings are relatively high, despite the relatively shallow permafrost.

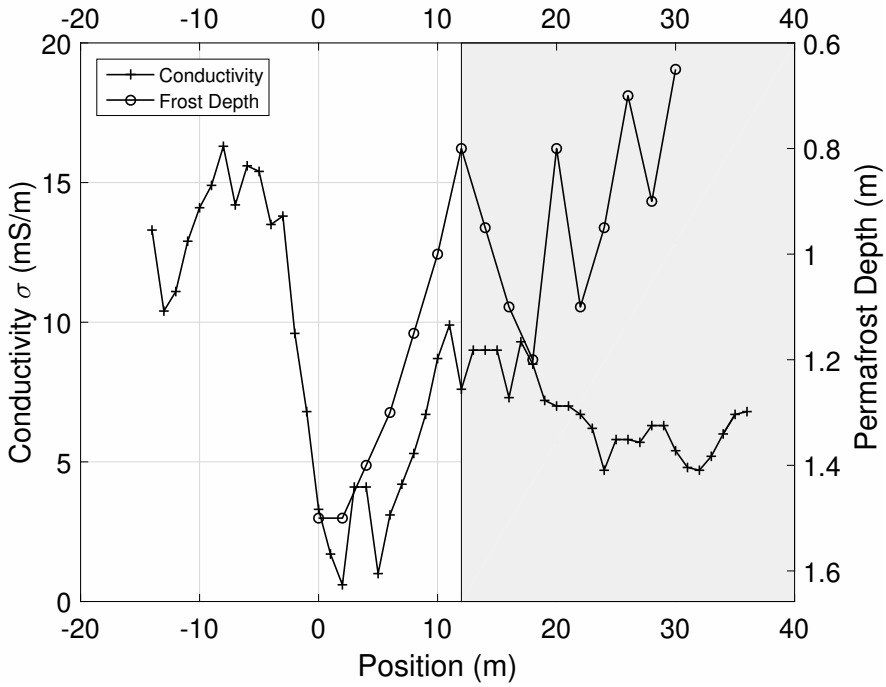

Figure 5.12: Electrical conductivity against permafrost probe measurements. Line 001 Configuration: EM-34, vertical dipole, 10 meter separation.

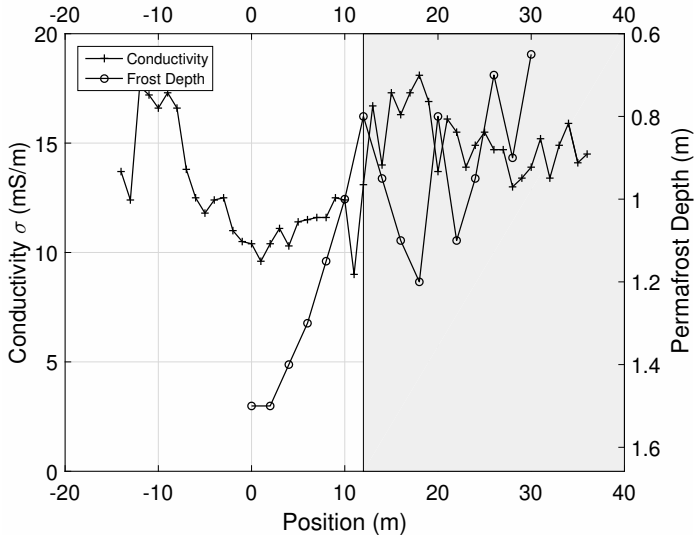

Figure 5.13: Electrical conductivity against permafrost probe measurements. Line 001 Configuration: EM-34, vertical dipole, 20 meter separation. The gray shaded area represents the vegetated/forested area.

Line 002

Only one EMI survey was performed on Line 002, since the wooded region was too densely vegetated. The survey was in the horizontal dipole configuration, and the coil separation was 10 meters. Based on the electromagnetic measurements, there is a shift in modality of the curve at approximately 10 meters, which would imply that the GCM detect the vertical change of the permafrost table. Again, the permafrost probe measurements of the plunging permafrost table is lagged behind the electrical measurements.

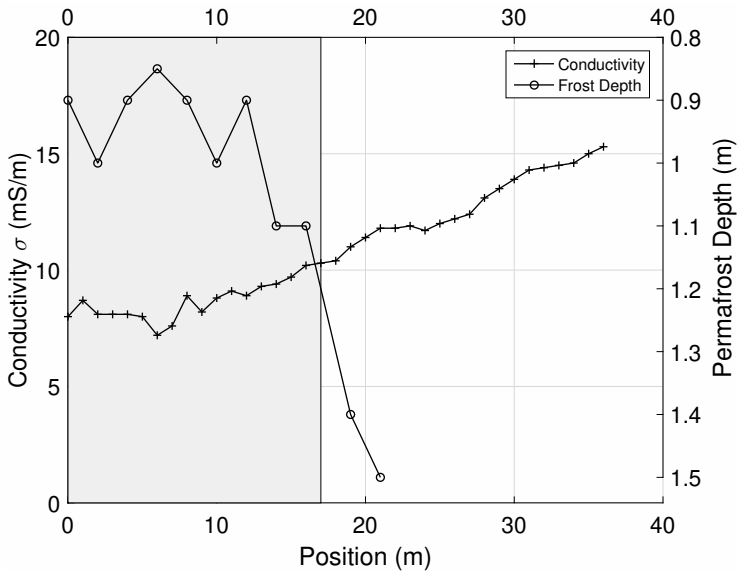

Figure 5.14: Electrical conductivity against permafrost probe measurements. Line 002 Configuration: EM-34, horizontal dipole, 10 meter separation. The gray shaded area represents the vegetated/forested area.

Line 004

Figures 5.15a to 5.16c show very similar trends. As the permafrost probe measurements show a deepening of the permafrost table, the electromagnetic measurements increase accordingly. Compared to lines 001 and 002, the slope of the electromagnetic measurements on Line 004 is steeper, which could be potentially due to a steeper slope of the permafrost table as it plunges. Similarly, the permafrost table plunge as measured by the permafrost probe lags behind the modality shift of the electromagnetic measurements.

Furthermore, the change in modality of the electromagnetic curves occur at approximately the same position. There is a slight offset between the electromagnetic measurements collected by the EM-31 and EM-34 equipment. The modal shift lag could potentially help calculate the slope of the permafrost table, non-invasively in a subsequent study.

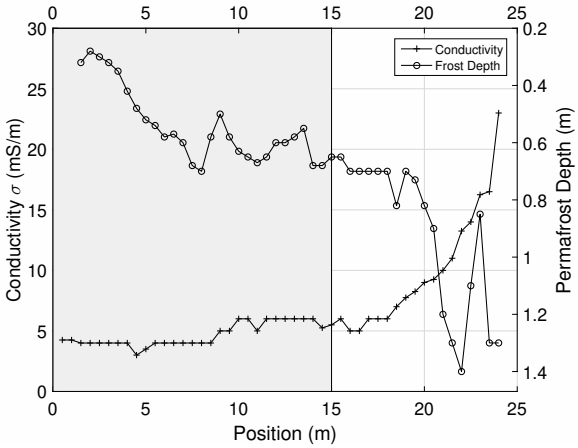

(a) Electrical conductivity against permafrost probe measurements. Line 004 Configuration: EM-31, horizontal dipole. The gray shaded area represents the vegetated/forested area.

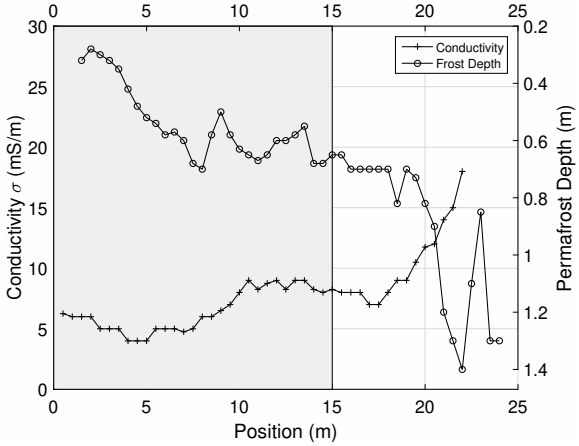

(b) Electrical conductivity against permafrost probe measurements. Line 004 Configuration: EM-31, horizontal dipole, 1 meter above ground. The gray shaded area represents the vegetated/forested area.

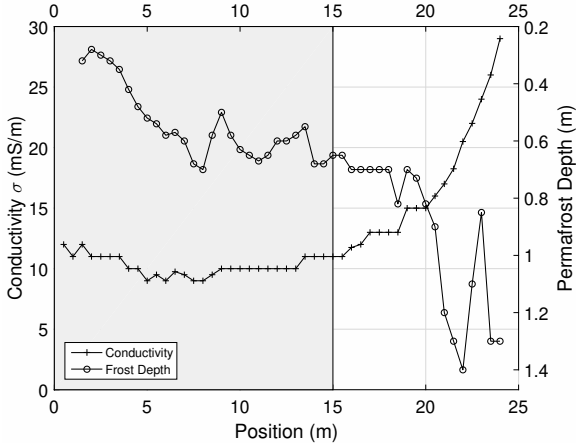

(c) Electrical conductivity against permafrost probe measurements. Line 004 Configuration: EM-31, vertical dipole. The gray shaded area represents the vegetated/forested area.

Figure 5.15: Electrical conductivity plotted against permafrost probe measurements for Line 004. [1 of 2]

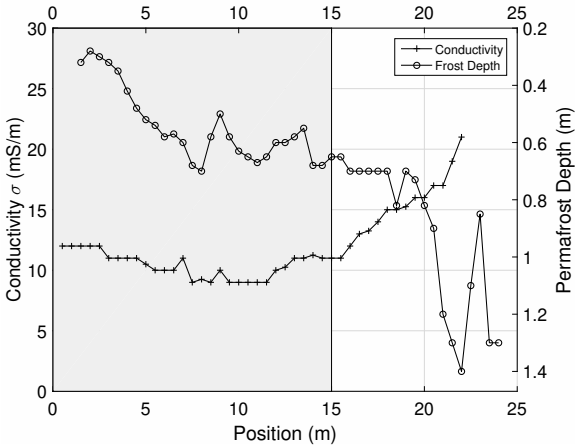

(a) Electrical conductivity against permafrost probe measurements. Line 004 Configuration: EM-31, vertical dipole, 1 meter above ground. The gray shaded area represents the vegetated/forested area.

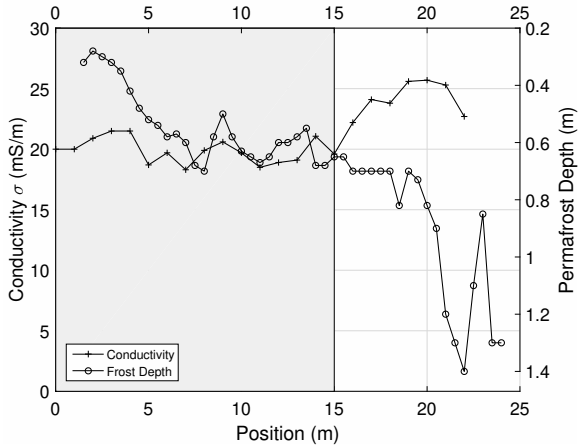

(b) Electrical conductivity against permafrost probe measurements. Line 004 Configuration: EM-34, vertical dipole, 10 meter separation. The gray shaded area represents the vegetated/forested area.

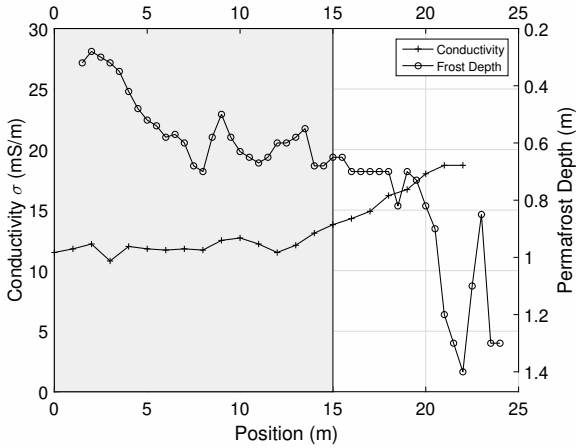

(c) Electrical conductivity against permafrost probe measurements. Line 004 Configuration: EM-34, horizontal dipole, 10 meter separation. The gray shaded area represents the vegetated/forested area.

Figure 5.16: Electrical conductivity plotted against permafrost probe measurements for Line 004. [2 of 2]

5.3.4 Joint Interpretation of EMI/Probe Data

It is clear in figures 5.9 to 5.16c that as increasing measurements of the permafrost probe, indicating a deepening on the permafrost table, that the electromagnetic measurements also indicate a correlative increase as well. Based on the visual assessment of the data, there is an evident background to the electromagnetic measurements, and that the background electrical conductivity is lower than the conductivity measurements upon transiting over the transition zone.

Examining the EMI and permafrost data concurrently, there is a spatial correlation between the permafrost table plunge and a conductivity threshold. On average, setting a conductivity threshold of 5 mS/m above the background conductivity lined up fairly well with the data.

5.3.5 Joint Interpretation of EMI/ERT Data

The ERT data has been inverted to show resistivity as a function of depth, which effectively displays the location of the permafrost in the ground. The EMI data on the other hand provides insights on the lateral distribution of the permafrost, such that it can measure the increase in conductivity as a result of a plunging permafrost table. The interpreted ERT data correlates well with the permafrost probe data. The EMI data was interpreted against the permafrost probe data, demonstrating a correlation between the plunging permafrost table, and an increasing electromagnetic measurement.

The rise of the measured conductivity by the GCM showed a lateral lag relative to the coil spacing and orientation. Along the survey transect, the shorter coil spacing would manifest a rising conductivity reading and as the survey progressed along the transect, the larger coil spacings (EM-34) would begin to show a rising conductivity. The lag is similar to the distance between active electrodes of the ERT. The greater the distance between electrodes, the deeper the measurement. Therefore, the electromagnetic survey could, at the very least, be a provisionally quantitative method to determine the slope of the plunging permafrost table.

5.3.6 Error Estimation

The error in the ERT and EMI data was analysed by benchmarking the electrical data against the permafrost probe data, which is considered to be our ground truthing. The error analysis will be evaluated for both directly estimating permafrost depth (vertical error) and estimating the location at which the permafrost plunges (lateral error). First, the degree of error in the depth of the permafrost as reported using the ERT discontinuity will be estimated from the difference between the depth measured by the permafrost probe and the resistivity boundary of the electrical resistivity tomography pseudosection. This provide some bounds upon the potential errors in the ERT results in the vertical direction. A second analysis will examine the various methods that determine the point at which the permafrost table begins to plunge. This will provide an estimate of the likely degree of error in the horizontal direction.

Electrical Resistivity Tomography Error Estimation

The vertical uncertainty is calculated based on the difference in interpreted ERT depth to permafrost table and the permafrost probe measurement.

$$\delta Z_{\text{upper}} = Z_1\text{upper} - Z_2\text{probe} \tag{5.1}$$

$$\delta Z_{\text{lower}} = Z_1\text{lower} - Z_2\text{probe} \tag{5.2}$$

$$\delta Z_{\text{middle}} = Z_1\text{middle} - Z_2\text{probe} \tag{5.3}$$

where Z_1 is the interpreted permafrost depth from the ERT pseudosection and Z_2 is the permafrost probe measurement.

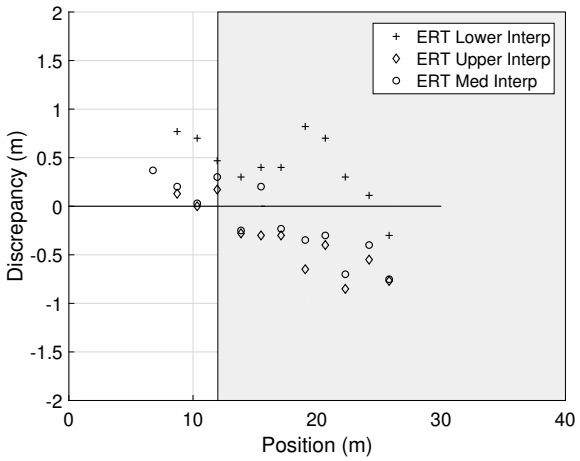

(a) Estimated discrepancy between ERT permafrost depth estimate and permafrost probe measurements. Line 001. The gray shaded area represents the vegetated/forested area.

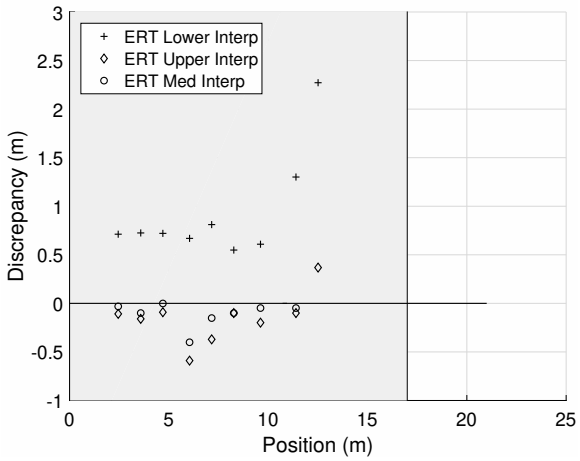

(b) Estimated discrepancy between ERT permafrost depth estimate and permafrost probe measurements. Line 002. The gray shaded area represents the vegetated/forested area.

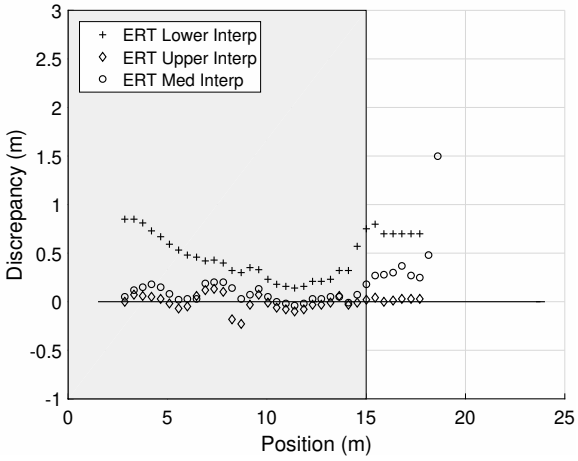

(c) Estimated discrepancy between ERT permafrost depth estimate and permafrost probe measurements. Line 004. The gray shaded area represents the vegetated/forested area.

Figure 5.17: Estimated discrepancy of ERT permafrost depth estimates versus permafrost probe measurements.

Vertical Error Estimation:

Line 001 : Refer to Figure 5.17a. The uncertainty of the ERT results is greater when the lower bound of the interpreted permafrost table is calculated against the permafrost probe data. However, the uncertainty lowers at the edge of the wooded area and near the 25 meter position. Conversely, the upper and middle interpretations showed little uncertainty, however the uncertainty rose further into the wooded area.

Line 002 : Refer to Figure 5.17b. Similar to Line 001, Line 002 shows very little uncertainty for the upper and middle ERT interpreted depths to the permafrost table. There is a noticeably higher uncertainty when isolating the lower depth to permafrost interpretation. Both uncertainties climb around the 12 meter position.

Line 004 : Refer to Figure 5.17c. The uncertainty for the upper and middle ERT interpretations are fairly constant. The lower interpretation shows mild convergence with the upper and middle interpretations at the 8 meter position. The uncertainty of the lower ERT interpretation rises again near the 14 meter position.

Based on the vertical uncertainty analysis, the ERT-based depth to permafrost interpretation holds some certainty when compared against the permafrost probe. However, it is very clear from this analysis that the upper bound of the resistivity plateau (ERT Upper Interp) is significantly more correlative with the permafrost probe measurements compared to the middle and lower interpretations.

Horizontal Error Estimation:

Line 001 : The ERT was marginally capable of defining the jaggedness of the permafrost probe measurements. The permafrost table plateaus in the ERT pseudosection where the permafrost probe measurements spike at 12 and 20 meters. The EMI data all has various responses to the permafrost. The EM-31 lines up well with the plunging permafrost table. The EM-34 at with a 10 meters coil separation shows little sensitivity to the changes, the EM-34 at 20 meters coil separate shows even less meaningful variation. It is not possible to calculate the vertical uncertainty of the EM-34 since the data does not show anything

Table 5.1: Mean error estimation of lines 001, 002, and 004 based the vertical difference between the permafrost probe measurements, and the interpreted ERT permafrost table at the low, median and high boundaries.

Line Number	Mean Error Upper(m)	Mean Error Lower(m)	Mean Error Median(m)
Line 001	-0.3455	0.4245	-0.1567
Line 002	-0.1500	0.9294	-0.1100
Line 004	-0.0032	0.4794	-0.1628

significant. Some of the data collected (i.e. EM-34, V.Dipole, 20m; EM-34, V.Dipole, 10m).

Line 002 : The ERT data and permafrost probe measurements match up well with approximately a 1 meter uncertainty. The permafrost has a shallow downward gradient near the edge of the tree clearing, and drops off quickly. Both gradients are measured accurately with the ERT system. The EMI however shows significant uncertainty since the edge of the higher permafrost table is not very well defined. However, recalling the principles of EMI, the increase in conductivity lines up well with the superposition of the receiver coil on the deepening permafrost. The permafrost and ERT lag the EMI measurements by approximately 10 meters, which is the coil separation we selected for the EM-34 system on this line.

Line 004 : The ERT data was with the permafrost probe data with some discrepancy. There is a zone of slightly higher resistivity at the 21 meter position. The permafrost probe intercepted an object at the 23 meter position, however it was not fully confirmed whether it not it was permafrost. The initial assumption was that the zone could be hard clay, however given its resistivity response, we are more certain that it could be permafrost, or ice. The initial drop in the permafrost table lines up well between the two datasets. The small rise in permafrost is also noticeable in the ERT data. The EMI data does not vary much with the smaller changes in the permafrost probe data, however, it is clear that the smaller system (EM-31) detects the permafrost thaw before the larger (EM-34) system. The EM-34 aligns the better with the permafrost probe data. The discrepancy between the EM-31 and probe data is approximately 5 meters, the EM-34 has a discrepancy of approximately 2 meters.

Electromagnetic Induction Error Estimation

The electromagnetic induction measurements have been plotted against the permafrost depths measured using the permafrost probe. The R^2 values are variable throughout this estimation, and do not demonstrate much certainty in the use of EMI as a proxy to measure the depth of the permafrost table. Note that, the units of the permafrost probe measurements ans conductivity are different, and that the error estimation did not include any consideration for proportionality between both values, as this was not part of the research.

Since there was no inversion performed on the electromagnetic data, it is unclear if there is any reliability in the vertical change in conductivity proportional to the permafrost table depth. This was, however, much more clearly defined in the ERT pseudosections. That being said, based purely on the change in conductivity in the horizontal direction, although noisy, an evident rise in conductivity is perceived, and can be correlated to the ERT pseudosection, and subsequently to the permafrost probe measurements.

Table 5.2: Calculated approximate R^2 values estimating the error between the electromagnetic induction measurements, and permafrost probe measurements.

Survey Line	**Survey Configuration**	$\approx R^2$
Line 001	MW04T EM-31	0.86
Line 001	MW04T EM-34 (Horizontal Dipole 10m)	0.77
Line 001	MW04T EM-34 (Horizontal Dipole 20m)	0.84
Line 001	MW04T EM-34 (Vertical Dipole 10m)	0.44
Line 001	MW04T EM-34 (Vertical Dipole 20m)	0.31
Line 002	MW04T EM-34 (Horizontal Dipole 10m)	0.80
Line 004	Marg Lake EM-31 (Vertical Dipole)	0.63
Line 004	Marg Lake EM-31 (Vertical Dipole + 1m altitude)	0.64
Line 004	Marg Lake EM-31 (Horizontal Dipole)	0.83
Line 004	Marg Lake EM-31 (Horizontal Dipole + 1m altitude)	0.73
Line 004	Marg Lake EM-34 (Vertical Dipole 10m)	0.63
Line 004	Marg Lake EM-34 (Horizontal Dipole 10m)	0.82

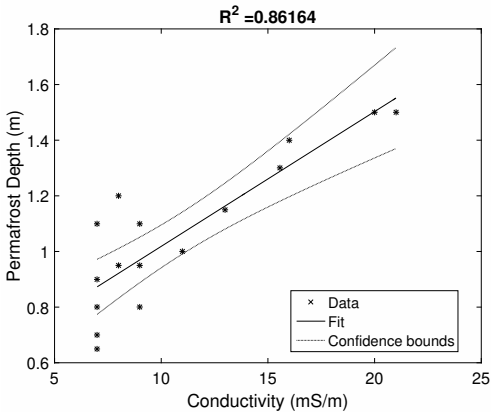

(a) Line 001 - MW04T EM-31 conductivity versus permafrost depth measured by permafrost probe. Best fit line applied with 95 percent confidence interval bounds.

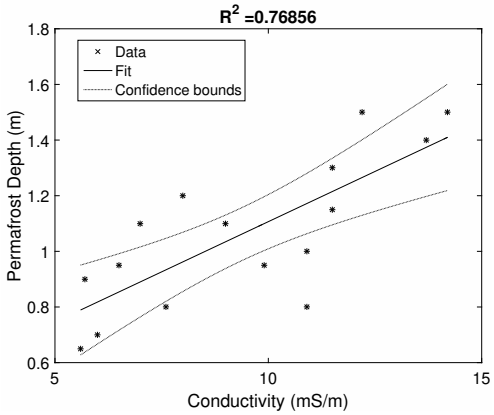

(b) Line 001 - MW04T EM-34 (Horizontal Dipole 10m) conductivity versus permafrost depth measured by permafrost probe. Best fit line applied with 95 percent confidence interval bounds.

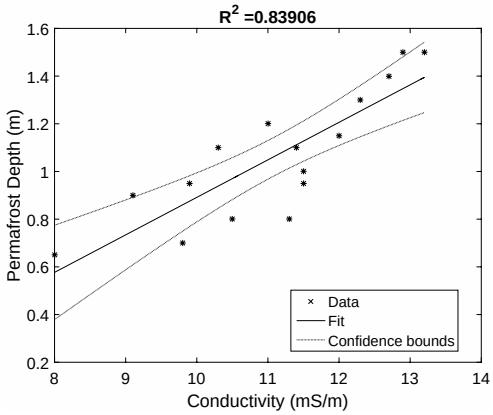

(c) Line 001 - MW04T EM-34 (Horizontal Dipole 20m) conductivity versus permafrost depth measured by permafrost probe. Best fit line applied with 95 percent confidence interval bounds.

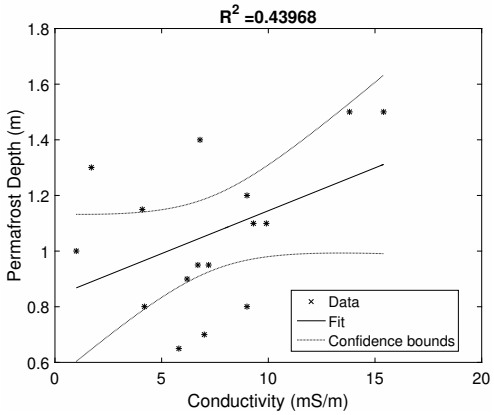

(d) Line 001 - MW04T EM-34 (Vertical Dipole 10m) conductivity versus permafrost depth measured by permafrost probe. Best fit line applied with 95 percent confidence interval bounds.

Figure 5.18: Error estimates of EMI measurements along Line 001.

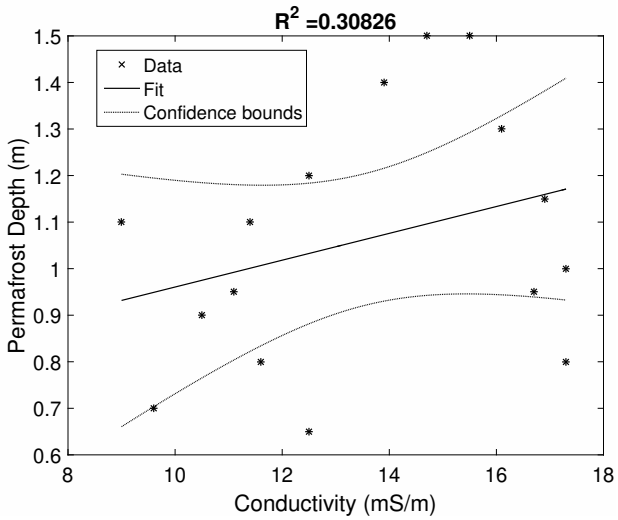

Figure 5.19: Line 001 - MW04T EM-34 (Vertical Dipole 20m) conductivity versus permafrost depth measured by permafrost probe. Best fit line applied with 95 percent confidence interval bounds.

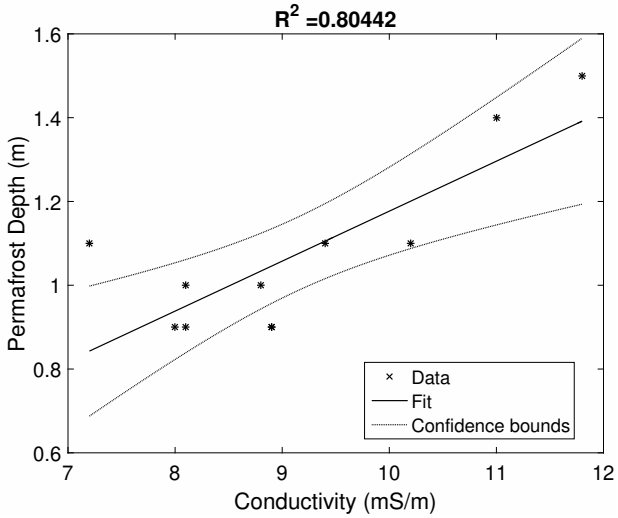

Figure 5.20: Line 002 - MW04T EM-34 (Horizontal Dipole 10m) conductivity versus permafrost depth measured by permafrost probe. Best fit line applied with 95 percent confidence interval bounds.

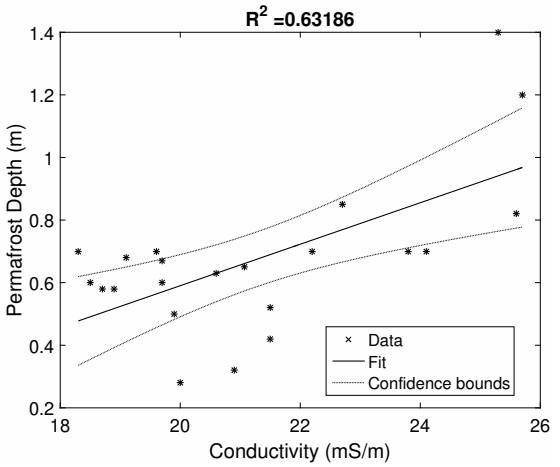

(a) Line 004 - Marg Lake EM-31 (Vertical Dipole) conductivity versus permafrost depth measured by permafrost probe. Best fit line applied with 95 percent confidence interval bounds.

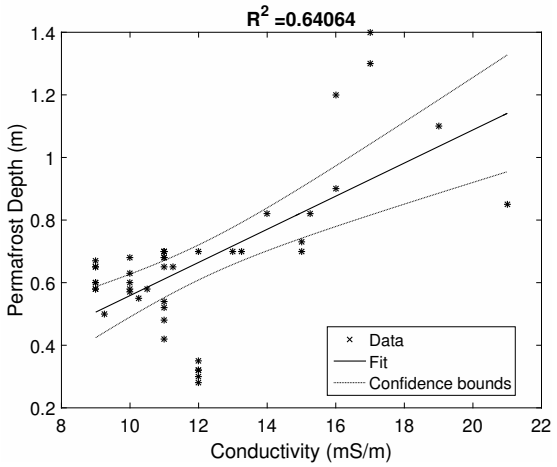

(b) Line 004 - Marg Lake EM-31 (Vertical Dipole + 1m altitude) conductivity versus permafrost depth measured by permafrost probe. Best fit line applied with 95 percent confidence interval bounds.

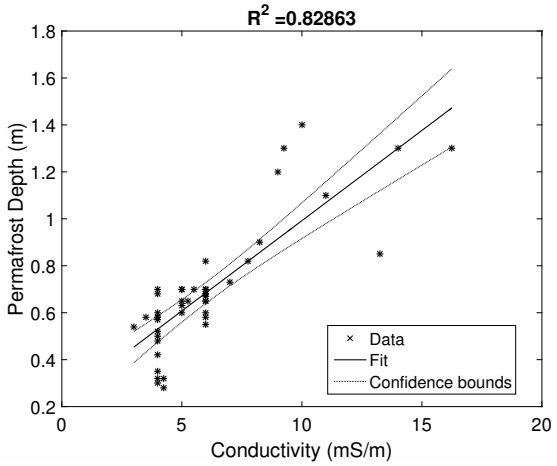

(c) LLine 004 - Marg Lake EM-31 (Horizontal Dipole) conductivity versus permafrost depth measured by permafrost probe. Best fit line applied with 95 percent confidence interval bounds.

Figure 5.21: Error estimates of EMI measurements along Line 004. [1 of 2]

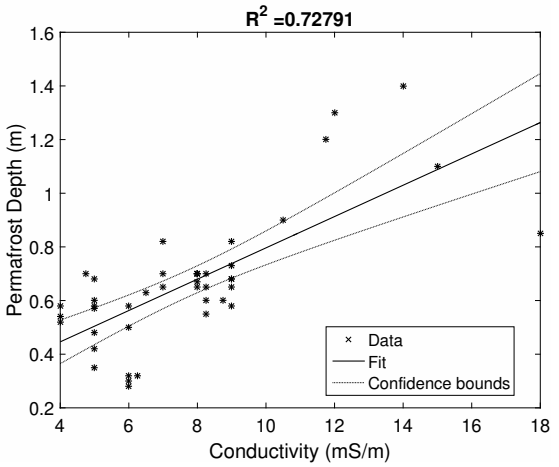

(a) Line 004 - Marg Lake EM-31 (Horizontal Dipole + 1m altitude) conductivity versus permafrost depth measured by permafrost probe. Best fit line applied with 95 percent confidence interval bounds.

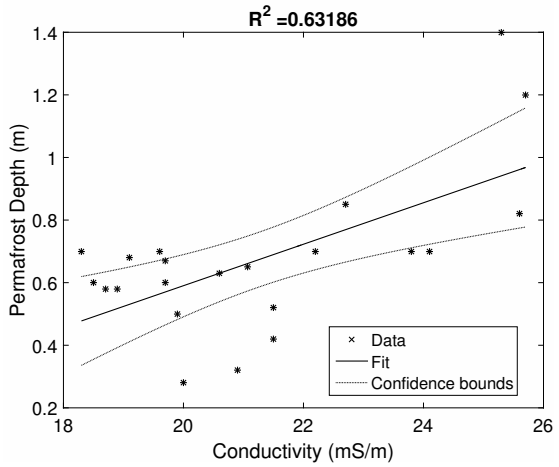

(b) Line 004 - Marg Lake EM-34 (Vertical Dipole 10m) conductivity versus permafrost depth measured by permafrost probe. Best fit line applied with 95 percent confidence interval bounds.

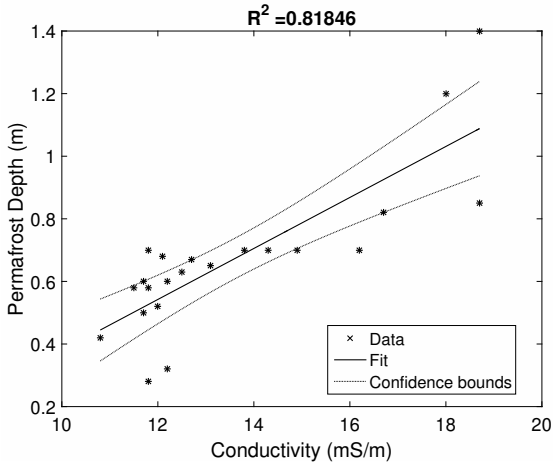

(c) Line 004 - Marg Lake EM-34 (Horizontal Dipole 10m) conductivity versus permafrost depth measured by permafrost probe. Best fit line applied with 95 percent confidence interval bounds.

Figure 5.22: Error estimates of EMI measurements along Line 004. [2 of 2]

Chapter 6

Conclusions

The findings in this study demonstrate that electrical resistivity tomography (ERT) is a suitable method to determine the characteristics of permafrost in soils where topomorphological and surface hydrological features exist. The work also used ground conductivity meter (GCM), which measured the conductivity of the soil along three principal survey lines. The data recorded by the ERT and EMI systems showed that by the use of geophysical instruments, one can gather information on the nature of subsurface permafrost in a quick and efficient manner. The results as outlined in the former sections show that these methods can be used to estimate the integrity of the permafrost in climate-sensitive regions, such as the Canadian Arctic. This method can be used to better understand the impact of human development in Northern Cold Regions, where activities such as clear cutting of trees, or road construction significantly influence the distribution of permafrost in the area.

Based on the results, ERT showed more accurate and relevant data than the EMI method. The ERT system was capable of determining the depth of the permafrost table with an accuracy less than 0.2 meters on average. Since the research was performed in the Sahtu region of the Northwest Territories, land access and manoeuvrability was limited. Therefore, in addition to using the ERT method, the work also incorporated the use of the EMI geophysical method. Unlike ERT, EMI is wholly non-invasive, and requires no physical ground coupling, making this a more agile system. Additionally, the ERT system as a whole is very heavy, and generally requires two individuals to safely ground-transport and install/operate. The mobilization of the EMI system on the other hand is quite rapid, and depending on the system being used, a GCM can be deployed by only one person. Furthermore, since this method is lightweight and requires no physical ground coupling,

this method can be deployed on a utility vehicle or snow machine.

Based on the analysis of this study, one can determine a change in permafrost table depth using EMI. Compared to the ERT, it is not possible to accurately determine the depth of the permafrost table without inverting the EMI data. The integrity of the lateral distribution of permafrost was determined by identifying a background conductivity where permafrost was shallow, and comparing it to a positive slope showing a rise in conductivity. Based on the observations of the data, and correlating the EMI measurements with the permafrost probe measurements, a threshold of 5 mS/m was set, which lined up fairly well with the plunging permafrost. Unfortunately, the data collection only took place over four days, limited data was collected in the field. Therefore, the conclusions made in this study show the potential use of these methods, and that much more data should be collected to increase our faith in the methods.

This work is relevant to the work performed by engineers, who rely on easily accessible measurements and information, in an efficient and affordable fashion, to best design infrastructure and other development projects. As mentioned previously, the use of this technique is valuable to engineers wishing to evaluate and monitor the geotechnical properties of a soil that is permafrost rich.

Future research in this field would be to merge remote sensing data of vegetation and soil topology from satellites, and combine these data with RPAS-based remote sensing and geophysical methods to better understand the climate dynamics of these regions. In the literature review, we have seen work performed on a large scale using helicopter based electromagnetic induction, however, so far there is still no reliable work on the smaller scale to address more localized engineering problems.

From the results of this work, the electrical responses (conductivity/resistivity) are proportional and sensitive to the permafrost content within the soil. Measurements taken by the permafrost probe showed a deepening of the permafrost table depth at the edge of the tree line entering into a clear cut area. The same trend was noted near the shoreline of a lake. Both instances inferred two things: 1) human activity in permafrost regions have an impact on the integrity of the permafrost, and; 2) surface features such as tree clearings and lakes can be indicators of permafrost thaw. Therefore, based on these two premises, two electrical methods were deployed to determine their efficiency.

Electrical resistivity tomography and electromagnetic induction surveys were conducted on the same lines as the permafrost probe. The results showed corroboration between the measurements of the permafrost probe and the electrical methods. The smaller electromagnetic system (Geonics EM-31) managed to determine laterally where the permafrost thaw occurred. This confirmed that a small-scaled electromagnetic system can pick up near surface permafrost discontinuities adjacent to laterally changing surface features.

The research here serves as a proof of concept for further research concerning the use of non-ground-coupled geophysical methods to better estimate the extent of permafrost thaw related to dynamic processes, whether they be anthropogenic or naturally occurring. The next steps are to develop an RPAS-based system that is capable of integrating various bands of geophysical and remote sensing data into one composite image using computer vision to more efficiently understand subsurface soils properties related to permafrost processes. Additionally, these classical geophysical methods have been used extensively in agriculture, however making them more efficient is necessary to help boost crop yield and improve farming practices. The understanding of small-scaled geophysical techniques and the increasingly developed RPAS market, RPAS-based methods will soon become commonplace in the engineering and geological research landscape.

References

[1] Arun Agrawal. Dismantling the Divide Between Indigenous and Scientific Knowledge. *Development and Change*, 26(3):413–439, 1995.

[2] M. M. Burgess and S. L. Smith. Shallow ground temperatures. *Bulletin of the Geological Survey of Canada*, (547):89–103, 2001.

[3] Ryan F Connon, William L Quinton, James R Craig, and Masaki Hayashi. Changing hydrologic connectivity due to permafrost thaw in the lower Liard River valley, NWT, Canada. *Hydrological Processes*, 28(May):4163–4178, 2014.

[4] S. Lawrence Dingman and Fleetwood R. Koutz. Relations among Vegetation, Permafrost, and Potential Insolation in Central Alaska. *Arctic and Alpine Research*, 6(1):37–47, 1974.

[5] Maria Engström and Bo Nordell. Temperature-driven groundwater convection in cold climates. *Hydrogeology Journal*, 24:1245 – 1253, 2016.

[6] Kotaro Fukui, Toshio Sone, Jorge A. Strelin, Cesar A. Torielli, Junko Mori, and Yoshiyuki Fujii. Dynamics and GPR stratigraphy of a polar rock glacier on James Ross Island, Antarctic Peninsula. *Journal of Glaciology*, 54(186):445–451, 2008.

[7] Stephan Gruber, Martin Hoelzle, and Wilfried Haeberli. Permafrost thaw and destabilization of Alpine rock walls in the hot summer of 2003. *Geophysical Research Letters*, 31(13):1–4, 2004.

[8] A Kääb, C Huggel, L Fischer, S Guex, F Paul, I Roer, N Salzmann, K Schmutz, D Schneider, A Kääb, C Huggel, L Fischer, S Guex, and F Paul. Remote sensing of glacier- and permafrost-related hazards in high mountains : an overview To cite this version : HAL Id : hal-00301627 Remote sensing of glacier- and permafrost-related hazards in high mountains : an overview. *Natural Hazards and Earth System Sciences*, 5:527–554, 2005.

[9] David M Lawrence and Andrew G Slater. A projection of severe near-surface permafrost degradation during the 21st century. *Geophysical Research Letters*, 32(December):1–5, 2005.

[10] Alastair F Mcclymont, Masaki Hayashi, Laurence R Bentley, and Brendan S Christensen. Geophysical imaging and thermal modeling of subsurface morphology and thaw evolution of discontinuous permafrost. *Journal of Geophysical*, 118:1826–1837, 2013.

[11] Gerald K. Moore. Ground-Water Applications of Remote Sensing. Technical report, 1982.

[12] T Nguyen, C. R. Burn, D. J. King, and S. L. Smith. Estimating the Extent of Near-surface Permafrost using Remote Sensing, Mackenzie Delta, Northwest Territories. *Permafrost and Periglacial Processes*, 20:141–153, 2009.

[13] T. E. Osterkamp and C. R. Burn. Permafrost. In *Encyclopedia of Atmospheric Sciences*, chapter 11, pages 1717–1729. 2003.

[14] Priyanka Pandey, Tom Gleeson, and Michel Baraer. Toward quantifying discrete groundwater discharge from frozen seepage faces using thermal infrared images. *Geophysical Research Letters*, 40(January):123–127, 2013.

[15] Alan J. Parkinson and Birgitta Evengård. Climate change, its impact on human health in the Arctic and the public health response to threats of emerging infectious diseases. *Global Health Action*, 2(1):0–3, 2009.

[16] W. G. Rees, M. Williams, and P. Vitebsky. Mapping land cover change in a reindeer herding area of the Russian arctic using Landsat TM and ETM+ imagery and indigenous knowledge. *Remote Sensing of Environment*, 85(4):441–452, 2003.

[17] S L Smith, T Nguyen, D W Riseborough, M Ednie, S Ye, and J Chartrand. Baseline geotechnical and permafrost data from new field sites established in the Mackenzie corridor south of Norman Wells , Northwest Territories Geological Survey of Canada Current Research 2010-2 Baseline geotechnical and permafrost data from new field. *Geological Survey of Canada, Current Research 2010-12*, 2010.

[18] M Stendel and J H Christensen. Impact of global warming on permafrost conditions in a coupled GCM. *Geophysical Research Letters*, 29(13):5–8, 2002.

[19] J. P. Texier and P. Bertran. Données Nouvelles sur la Présence d'un Pergélisol en Aquitaine au cours des Dernières Glaciations. *Permafrost and Periglacial Processes*, 4(3):183–198, 1993.

[20] Daniel Vonder and Christian Hauck. Mapping of mountain permafrost using geophysical methods. *Progress in Physical Geography*, 26(4):643–660, 2002.

[21] P Wainstein, B Moorman, and Ken Whitehead. Importance of Glacier-Permafrost Interactions in the Preservation of a Proglacial Icing: Fountain Glacier, Bylot Island, Canada. *Ninth International Conference on Permafrost*, (August):1–6, 2008.

[22] Michelle A. Walvoord and Barret L. Kurylyk. Hydrologic Impacts of Thawing Permafrost—A Review. *Vadose Zone Journal*, 15(6):0, 2016.

[23] Michelle A. Walvoord, Clifford I. Voss, and Tristan P. Wellman. Influence of permafrost distribution on groundwater flow in the context of climate-driven permafrost thaw: Example from Yukon Flats Basin, Alaska, United States. *Water Resources Research*, 48(7):1–17, 2012.

[24] Shuangjie Wang, Jianbing Chen, Jinzhao Zhang, and Zhulong Li. Development of highway constructing technology in the permafrost region on the Qinghai-Tibet plateau. *Science in China, Series E: Technological Sciences*, 52(2):497–506, 2009.

[25] Xiqiang Wang, Rensheng Chen, and Yong Yang. Effects of Permafrost Degradation on the Hydrological Regime in the Source Regions of the Yangtze and Yellow Rivers, China. *Water*, 9(897):1 – 13, 2017.

[26] Nicole Wright, Masaki Hayashi, and William L Quinton. Spatial and temporal variations in active layer thawing and their implication on runoff generation in peat-covered permafrost terrain. *Water Resources Research*, 45(W05414):1–13, 2009.